SIAM J. Applied Dynamical Systems
Vol. 23, No. 1, pp. 641–667


# Spatio-temporal Dynamics in a Reaction-Diffusion Equation with Nonlocal Spatial Memory*

Shuyang Xue†, Yongli Song‡, and Hao Wang§

**Abstract.** To model a single-species cognitive movement, we formulate a reaction-diffusion equation with nonlocal spatial memory and investigate its dynamics. We explore the influence of the perceptual scale on the stability and Turing bifurcation. When the random diffusion is dominant, the perceptual scale does not affect the stability, but when the memory-based diffusion is dominant, there exist Turing bifurcations induced by the perceptual scale. Then the joint effect of the perceptual scale and the memory delay on the stability and spatio-temporal dynamics is investigated to show rich spatio-temporal dynamics via Turing–Hopf bifurcation and double Hopf bifurcation. Finally, we apply our analysis to an application and illustrate our theoretical results with numerical simulations.

**Key words.** advection-diffusion, memory, Turing bifurcation, Hopf bifurcation, Turing–Hopf bifurcation

**MSC codes.** 35B32, 35B36, 35B40, 35Q92, 92B05

**DOI.** 10.1137/22M1543860

## 1. Introduction.

Recently, there has been an increasing activity and interest in the study of reaction-diffusion equations with nonlocal advection. Nonlocal advection is a key process in a range of biological systems and is often used to describe biological aggregations such as fish schools, bird flocks, bacterial colonies, and insect swarms [2]. Mathematically, the nonlocal sensing of neighboring individuals leads to nonlocal advection terms [3, 9]. For the single population, the following nonlocal advection-diffusion model is often used to model the movement of individuals in response to the presence of others:

$$\frac{\partial u}{\partial t} = d_1 \frac{\partial^2 u}{\partial x^2} + d_2 \frac{\partial}{\partial x}\left( u \frac{\partial}{\partial x}(K * u)\right) + f(u),\ x \in \Omega, t > 0, \tag{1.1}$$

where $\Omega$ is a spatial habitat of the population, and $u(x,t)$ is locational density of population $u$ at location $x$ and time $t$. The first term on the right-hand side of (1.1) describes the random motion of the population, and $d_1 > 0$ is the corresponding diffusion coefficient (also known as the random diffusion rate). The second term on the right-hand side of (1.1) describes the

*Received by the editors December 29, 2022; accepted for publication (in revised form) by T. Kolokolnikov December 5, 2023; published electronically February 21, 2024.
https://doi.org/10.1137/22M1543860
**Funding:** This work was partially supported by grants from Zhejiang Provincial Natural Science Foundation of China (LZ23A010001), National Natural Science Foundation of China (12371166 and 12071105), and Natural Sciences and Engineering Research Council of Canada (Discovery grant RGPIN-2020-03911 and Accelerator grant RGPAS-2020-00090).
†School of Mathematics, Hangzhou Normal University, Hangzhou, 311121, China, and School of Mathematics and Statistics, Central South University, Changsha 410083, China (20223057@hznu.edu.cn).
‡School of Mathematics, Hangzhou Normal University, Hangzhou, 311121, China (songyl@hznu.edu.cn).
§Corresponding author. Department of Mathematical and Statistical Sciences & Interdisciplinary Lab for Mathematical Ecology and Epidemiology, University of Alberta, Edmonton, AB T6G 2G1, Canada (hao8@ualberta.ca).

directional motion (gradient following movement) of the population. $d_2 \in \mathbb{R}$ is the advection rate. $K * u$ is the convolution of $u$ with a spatial kernel. The third term $f(u)$ on the right-hand side of (1.1) describes the evolution of the population such as the growth and the death. Equation (1.1) appears in the mathematical modeling of cell population dynamics [18, 3] and has also been introduced in crowd dynamics [2]. We also refer the reader to Morale, Capasso, and Oelschlager [17] and Mogilner and Edelstein-Keshet [16] for the derivation of the nonlocal advection terms. Depending on the kernel function, the stability and instability of the unique homogeneous positive steady state of (1.1) have been investigated in [6]. For $d_1 = 0$ the global asymptotic behavior of (1.1) for kernels with positive Fourier transform has been dealt with in [7]. For the case of the discrete space, the asymptotically stable steady states of (1.1) have been studied via an energy functional approach [20]. For more significant mathematical results of this kind of nonlocal advection-diffusion equation such as classical questions of existence and uniqueness, pattern formation properties, and bifurcations, see [4, 11, 12, 31] and the good recent reviews [3, 5, 33].

A multispecies system with nonlocal advection diffusion has been recently proposed by Potts and Lewis [19] and slightly generalized by Giunta et al. [9]. In [9], the existence theorems for a class of nonlocal multispecies advection-diffusion models, with an arbitrary number of coexistent species, has been investigated, and global existence has been shown for models in $n = 1$ spatial dimension and local existence for $n > 1$. In [10], Giunta et al. developed methods for determining the qualitative structure of local minimum energy states of a multispecies nonlocal advection-diffusion models proposed in [9].

More recently, in order to describe the influence of spatial memory and cognition on animal movements, Shi et al. [24] incorporated cognition and memory of "clever" animals in the simplest and self-contained way and proposed the following so-called memory-based diffusion model to describe the diffusive spatial movement of the population with memory:

$$\begin{cases} \frac{\partial u}{\partial t} = d_1 \frac{\partial^2 u}{\partial x^2} + d_2 \frac{\partial}{\partial x}\left(u \frac{\partial}{\partial x}\left(u_\tau\right)\right) + f\left(u\right), & x \in \Omega, t > 0, \\ \frac{\partial u}{\partial \mathbf{n}} = 0, & x \in \partial\Omega, t > 0, \end{cases} \tag{1.2}$$

where $u_\tau = u(x, t-\tau)$, the delay $\tau \geq 0$ represents the averaged memory period, and $\frac{\partial u}{\partial \mathbf{n}}$ is the outer normal derivative of $u$ at $x \in \partial\Omega$. After the pioneering work by Shi et al. [24], there has been plenty of interest in studying the role of the spatial memory in animal movements (see, e.g., [1, 13, 14, 22, 23, 26, 28, 29, 32]). Among all of the above-mentioned research works, the memory-based diffusion is only related to the memory of a past particular moment $t - \tau$ at location $x$, which induces local discrete delay. Intuitively, this assumption is not reasonable since the spatial memories are often decaying in the animal's brains over time. In [15, 21], the memory-based diffusion is described by the so-called temporally distributed delay, which reflects the memory decay at past time at location $x$. However, it is more realistic to use a nonlocal distributed average of spatial memory because the temporal and spatial distributed delay reflects that the decay of spatial memory depends on time and the distance of past animal distributions from the decision-making individual [25]. In [25, 30], based on the assumption that the spatial memory is related to the memorized information during all the past times and the spatial distribution of the species, the spatio-temporal delay is introduced to describe the memory-based diffusion.

Since highly developed animals can acquire knowledge from individuals in their neighboring range, the spatial memory should reflect this spatial nonlocality. Motivated by this idea and the above works on memory-based diffusion, we consider a model in one periodic interval $(-L, L)$ with the following periodic boundary conditions:

$$\begin{cases} \frac{\partial u}{\partial t} = d_1 \frac{\partial^2 u}{\partial x^2} + d_2 \frac{\partial}{\partial x}\left(u \frac{\partial}{\partial x}(K_r * u_\tau)\right) + f(u), & x \in (-L, L), t > 0, \\ u(-L, t) = u(L, t), \quad u_x(-L, t) = u_x(L, t), & t > 0, \end{cases} \tag{1.3}$$

where

$$K_r * u_\tau = \int_{-L}^{L} K_r(x - y) u(y, t - \tau) dy, \tag{1.4}$$

and $K_r$ is chosen as the top-hat function as follows:

$$K_r(x) = \begin{cases} \frac{1}{2r}, & -r \le x \le r, \\ 0 & \text{otherwise.} \end{cases} \tag{1.5}$$

In model (1.3), we assume that animals collect information from their adjacent individuals at a particular past time and their current position, and the gradient of the past accumulated weighted spatial information of the population serves as the velocity in the advection term. The top-hat function (1.4) means that the animal can collect information equally a fixed distance $r$ away from its current location and cannot collect beyond that fixed distance. We call $r$ the animal's perceptual scale, which reflects the extent to which the animals can obtain information from the adjacent individuals. We would also like to mention that this kernel function (1.4) has often been used to characterize the nonlocal resource perception for another subject [8, 33].

In what follows, we refer the reader to $\tau$ and $d_2$ as the memory delay and memory diffusion rate, respectively. According to the periodic boundary conditions, in order for $K_r * u_\tau$ as defined by (1.4) to have reasonable definition for any $x \in (-L, L)$, we supplement the definition of $u(x, t)$ for $x \in [-L - r, -L] \cup [L, L + r]$ as follows:

$$\begin{cases} u(x, t) = u(x + 2L, t) & \text{for } x \in [-L - r, -L], \quad t \ge 0, \\ u(x, t) = u(x - 2L, t) & \text{for } x \in [L, L + r], \quad t \ge 0. \end{cases} \tag{1.6}$$

Notice that

$$\lim_{r \to 0^+} (K_r * u_\tau) = u(x, t - \tau).$$

Thus, if we allow $r = 0$ and set $(K_0 * u_\tau) = u(x, t - \tau)$, then (1.3) becomes the memory-based diffusion equation (1.2). If $\tau = 0$, then (1.3) becomes (1.1). Therefore, model (1.3) can be considered as the bridge between models (1.1) and (1.2). In this paper, we will investigate the influence of the forager's perceptual scale $r$ and the memory delay $\tau$ on the stability and the spatio-temporal dynamics of model (1.3).

In addition, noticing that $x - y \in [-r, r]$ for $y \in [x - r, x + r]$, it follows from (1.5) that

$$K_r * u_\tau = \int_{-L}^{L} K_r(x - y) u(y, t - \tau) dy = \frac{1}{2r} \int_{x-r}^{x+r} u(y, t - \tau) dy. \tag{1.7}$$

For $r = L$ and $x \in (-L, L)$, it follows from (1.6) that $\int_L^{L+x} u(y,t)dy = \int_{-L}^{-L+x} u(y,t)dy$ for any $t > 0$. And then, by (1.7), we have

$$
\begin{aligned}
K_L * u_\tau &= \frac{1}{2L}\int_{x-L}^{x+L} u(y, t-\tau)dy \\
&= \frac{1}{2L}\left(\int_{x-L}^{L} u(y,t-\tau)dy + \int_{L}^{L+x} u(y,t-\tau)dy\right) \\
&= \frac{1}{2L}\left(\int_{-L+x}^{L} u(y,t-\tau)dy + \int_{-L}^{-L+x} u(y,t-\tau)dy\right) \\
&= \frac{1}{2L}\int_{-L}^{L} u(y,t-\tau)dy.
\end{aligned} \tag{1.8}
$$

Obviously, from (1.8), $K_L * u_\tau$ is independent of $x$, which is the average value of $u(x, t-\tau)$ on the space $[-L, L]$. Thus, $\frac{\partial (K_L * u_\tau)}{\partial x} = 0$, and (1.3) becomes the classical reaction-diffusion equation $\frac{\partial u}{\partial t} = d_1 \frac{\partial^2 u}{\partial x^2} + f(u)$.

Thus, in this paper, we focus on the case of $r \in (0, L)$ and $\tau \geq 0$ and investigate the influence of $r$ and $\tau$ on the stability of (1.3) and the spatio-temporal patterns. For $d_2 < 0$, $r$ and $\tau$ do not affect stability. For $d_2 > 0$, there are complex dynamics induced by the perceptual scale and the memory delay. Our main findings are summarized as follows:

(i) If a memory delay does not exist (i.e., $\tau = 0$), then when the random diffusion is dominant, the perceptual scale $r$ does not affect the stability, but when the memory-based diffusion is dominant, the perceptual scale $r$ can lead to Turing bifurcation such that the positive constant steady state is unstable for small perceptual scale (no matter how small it is) and asymptotically stable for large perceptual scale;

(ii) If a memory delay exists (i.e., $\tau > 0$), then when the random diffusion is dominant, the perceptual scale $r$ and the memory delay $\tau$ also do not affect the stability; however, when the random diffusion rate and the memory-based diffusion rate satisfy certain relationships, Turing bifurcation, Hopf bifurcation, and Turing–Hopf bifurcation can occur with spatial patterns, periodic patterns, and spatio-temporal patterns and more complex dynamics.

The rest of the paper is organized as follows. In section 2, we study the well-posedness of solutions. In section 3, we first study the spectral properties of the linear operator, then investigate the influence of the forager's perceptual scale $r$ on the stability of (1.3) and the Turing bifurcation, and finally we study the joint effect of the forager's perceptual scale $r$ and memory delay $\tau$ on the stability of (1.3) and the Hopf bifurcation and Turing–Hopf bifurcation. In section 4, we apply the theoretical results to investigate the spatio-temporal dynamics of (1.3) with logistic growth and make some numerical simulations to illustrate the patterns. Finally, we summarize our paper with a discussion in section 5.

Throughout the paper, $\mathbb{N}$ represents the set of all positive integers, $\mathbb{N}_0 = \mathbb{N} \cup \{0\}$ represents the set of all nonnegative integers, and $\mathbb{Z}$ represents the set of all integers.

## 2. Well-posedness of solutions.

In this section, we first consider the well-posedness of solutions of (1.3) for appropriate initial function $\varphi(x,t), (x,t) \in (-L, L) \times [-\tau, 0]$. Assume that the initial function $\varphi(x,t)$ satisfies

$$\varphi(x,t)\in C^{2,\alpha}\left([-L,L]\times[-\tau,0]\right),\ \alpha\in(0,1), \tag{2.1}$$

and

$$\varphi(-L,t)=\varphi(L,t),\quad \varphi_x(-L,t)=\varphi_x(L,t),\ t\in[-\tau,0]. \tag{2.2}$$

The growth function $f(u)$ is assumed to satisfy

$$f(u)\in C^1\left([0,\infty),\mathbb{R}\right),\ f(0)=f(1)=0,\ f(u)<0 \text{ for } u>1. \tag{2.3}$$

For the kernel function defined by (1.7), if $u(x,t)\in C\left([-L,L]\times[-\tau,0]\right)$, then by (1.7) we have

$$\frac{\partial K_r * u_\tau}{\partial x}=\frac{1}{2r}(u(x+r,t)-u(x-r,t))\in C\left([-L,L]\times[-\tau,0]\right),$$

which implies that the smoothness of the convolution $K_r * u_\tau$ is better than the smoothness of $u$. In addition, notice that for $t\in[0,\tau]$, $u_\tau$ coincides with the initial function $\varphi(x,t-\tau)$. Therefore, if $\varphi(x,t)\in C^{2,\alpha}\left([-L,L]\times[-\tau,0]\right)$, then for $t\in[0,\tau]$, $v(x,t)=K_r * u_\tau\in C^{2,\alpha}\left([-L,L]\times[0,\tau]\right)$. Then, following the proof for Proposition 2.1 in [24], we have the following results for the well-posedness.

Proposition 2.1. *Assume that $d_1>0, d_2\in\mathbb{R}$ and $f(u)$ satisfies (2.3). Then, for the initial function $\varphi(x,t)$ satisfying (2.1) and (2.2) and the kernel function defined by (1.7), equation (1.3) possesses a unique solution $u(x,t)$ for $(x,t)\in[-L,L]\times[0,\infty)$, and $u(x,t)\in C^{2,1}\left([-L,L]\times[-\tau,0]\right)$. Moreover, if $\varphi(x,t)\geq 0(\not\equiv 0)$ for $(x,t)\in[-L,L]\times[-\tau,0]$, then $u(x,t)>0$ for $(x,t)\in[-L,L]\times[0,\infty)$.*

## 3. Spectral analysis, stability, and bifurcation analysis.

Assume that $u_*$ is a positive constant such that $f(u_*)=0$. Then, by (1.4) and (1.5), $u_*$ is a positive constant steady state of (1.3). The linearized equation of (1.3) at $u=u_*$ is

$$\begin{cases} \frac{\partial u}{\partial t}=d_1\frac{\partial^2 u}{\partial x^2}+\tilde{d}_2\frac{\partial^2}{\partial x^2}(K_r * u_\tau)+Au, & t>0,\ x\in(-L,L),\\ u(-L,t)=u(L,t),\quad u_x(-L,t)=u_x(L,t), & t\geq 0, \end{cases} \tag{3.1}$$

where $\tilde{d}_2=d_2u_*$, $A=f'(u_*)$.

### 3.1. Spectral analysis.

In this subsection, we first study some spectral properties of the linearized problem (3.1). Let

$$\mathcal{C}_L=C\left([-\tau,0],L^2(\Omega);\mathbb{C}\right),\ \mathcal{C}_H=C\left([-\tau,0],H^2(\Omega);\mathbb{C}\right)\subset\mathcal{C}_L.$$

We can rewrite (3.1) as the abstract ODE

$$\frac{d\phi}{dt}=\mathcal{L}(\phi), \tag{3.2}$$

where

$$\mathcal{L}(\phi)(\theta)=\begin{cases}\mathcal{A}\phi+A\phi(0), & \theta=0,\\ \dot{\phi}(\theta), & \theta\in[-\tau,0),\end{cases} \tag{3.3}$$

with

$$\mathcal{A}\phi = d_1\phi''(0) + \tilde{d}_2(K_r * \phi(-\tau))'', \ \mathrm{Dom}\mathcal{A} = \mathcal{C}_H, \tag{3.4}$$

where $\phi'' = \frac{\partial^2\phi}{\partial x^2}, \dot{\phi} = \frac{\partial\phi}{\partial t}$.

The domain of the operator $\mathcal{L}$ is determined by

$$\mathrm{Dom}(\mathcal{L}) = \left\{\dot{\phi} \in \mathcal{C}_L : \ \phi \in \mathcal{C}_H, \ \dot{\phi}(0) = \mathcal{A}\phi + A\phi(0)\right\}.$$

Lemma 3.1. *For $\Omega = (-L, L)$, the spectrum of the linear operator $\mathcal{L}$, denoted by $\sigma(\mathcal{L})$, only consists of the point spectrum $\sigma_P(\mathcal{L})$, the set of eigenvalues of $\mathcal{L}$, and one has*

$$\sigma(\mathcal{L}) = \sigma_P(\mathcal{L}) = \{\lambda_n : \ E(n, \tau, \lambda) = 0, \ n \in \mathbb{Z}\},$$

*where*

$$E(n, \tau, \lambda) = \lambda + \left(\frac{n\pi}{L}\right)^2 \left(d_1 + \tilde{d}_2 e^{-\lambda\tau} H(r, n\pi/L)\right) - A \tag{3.5}$$

*with*

$$H(r, n\pi/L) = \begin{cases} \frac{\sin(n\pi r/L)}{n\pi r/L}, & n \neq 0, \\ 1, & n = 0. \end{cases} \tag{3.6}$$

*Proof.* For $\Omega = (-L, L)$, introduce the inner product in $L^2(\Omega)$ as follows:

$$\langle \varphi, \psi \rangle = \frac{1}{2L} \int_{-L}^{L} \overline{\varphi(x)} \psi(x) dx \ \ \forall \varphi, \psi \in L^2(\Omega).$$

Then the corresponding norm on $L^2(\Omega)$ is induced by $\|\cdot\|_0$ and $L^2(\Omega)$ becomes the Hilbert space. The Hilbert bases for $L^2(\Omega)$ can be chosen as

$$\left\{e_n(x) = e^{\frac{in\pi x}{L}}, n \in \mathbb{Z}\right\}.$$

For each function $\varphi \in L^1(\Omega)$, its Fourier expansion is

$$\varphi = \sum_{n \in \mathbb{Z}} c_n(\varphi) e_n(x),$$

where $c_n(\varphi) = \langle e_n(x), \varphi \rangle$.

For given $\lambda \in \mathbb{C}$ and $g(\theta) \in \mathcal{C}_L$, assume that there exists $\phi(\theta) \in \mathrm{Dom}(\mathcal{L})$ such that

$$(\lambda I - \mathcal{L})\phi(\theta) = g(\theta). \tag{3.7}$$

It follows from (3.3) that for $\theta \in [-\tau, 0)$, $\mathcal{L}\phi(\theta) = \dot{\phi}(\theta)$, and then (3.7) becomes the following linear differential equation:

$$\dot{\phi}(\theta) = \lambda\phi(\theta) + g(\theta). \tag{3.8}$$

Solving (3.7) for the initial value $\phi(0) = b \in H^2(\Omega)$, we have

$$\phi(\theta) = e^{\lambda\theta} b + \int_0^\theta e^{\lambda(\theta-\xi)} g(\xi) d\xi, \tag{3.9}$$

where $b$ is a function to be determined such that it satisfies the equality

$$\dot{\phi}(0) = \mathcal{A}\phi + A\phi(0) \tag{3.10}$$

such that $\phi \in \mathrm{Dom}(\mathcal{L})$. In terms of (1.4), we have

$$K_r * (e_n(x)) = H(r, n\pi/L) e_n(x). \tag{3.11}$$

For $g(\theta) \equiv 0$ and $b = e_n(x)$, it is easy to see that the equation $(\lambda I - \mathcal{L}) e^{\lambda\theta} e_n(x) = 0$ if and only if there exists $\lambda \in \mathbb{C}$ such that $E(n, \tau, \lambda) = 0$. And, obviously, $\phi(\theta) = e^{\lambda\theta} e_n(x)$ satisfies (3.10). This implies that

$$\{\lambda_n : E(n, \tau, \lambda) = 0,\ n \in \mathbb{Z}\} \subset \sigma_P(\mathcal{L}). \tag{3.12}$$

For $g(\theta) \in \mathcal{C}_H$ and $g(\theta) \neq 0$, it follows from (3.9) that

$$\dot{\phi}(0) = \lambda\phi(0) + g(0). \tag{3.13}$$

Let $\eta(\theta) = \int_0^\theta e^{\lambda(\theta-\xi)} g(\xi) d\xi$ and notice that $\eta(0) = 0$. Then, from (3.4) and (3.11), we have

$$\mathcal{A}\eta(\theta) = \sum_{n\in\mathbb{Z}} c_n(\eta(-\tau)) H(r, n\pi/L) e_n(x). \tag{3.14}$$

According to (3.4), (3.9), (3.10), and (3.14), we have

$$\lambda c_n(b) + c_n(g(0)) = -n^2 \left(d_1 + \tilde{d}_2 e^{-\lambda\tau} H(r, n\pi/L)\right) c_n(b) + A c_n(b) + c_n(\eta(-\tau)) H(r, n\pi/L). \tag{3.15}$$

Therefore, for $\lambda \in \mathbb{C} \setminus \{\lambda_n, n \in \mathbb{Z}\}$, we have $\lambda - \lambda_n \neq 0$ and

$$c_n(b) = \frac{-c_n(g(0)) + c_n(\eta(-\tau)) H(r, \tau)}{\lambda - \lambda_n}.$$

Letting $b = \sum_{n\in\mathbb{Z}} c_n(b) e_n(x)$, then $\phi(\theta)$ defined by (3.9) is a unique solution of (3.7), provided that $\lambda \in \mathbb{C} \setminus \{\lambda_n, n \in \mathbb{Z}\}$. This means that

$$\mathbb{C} \setminus \{\lambda_n, n \in \mathbb{Z}\} \subset \rho(\mathcal{L}),$$

which, together with the fact that $\rho(\mathcal{L}) = \mathbb{C} \setminus \sigma(\mathcal{L})$, implies

$$\sigma_P(\lambda) \subset \sigma(\mathcal{L}) \subset \{\lambda_n, n \in \mathbb{Z}\}. \tag{3.16}$$

Combining (3.12) and (3.16), the proof is complete. ∎

Notice the fact that for the kernel function defined by (1.7), the smoothness of the convolution $K_r * u_\tau$ is better than the smoothness of $u$. Then, using arguments similar to those in [24], one can show that the solution operator defined by (3.2) possesses some compactness property. Therefore, the stability of the positive constant steady state $u = u_*$ is determined by the point spectrum $\sigma_P(\mathcal{L})$.

**3.2. Stability and bifurcation analysis.** From subsection 3.1, we know that the stability of the positive constant steady state $u = u_*$ of (1.3) is determined by the distribution of roots of the following characteristic equation:

$$\lambda + \left(\frac{n\pi}{L}\right)^2 \left(d_1 + \tilde{d}_2 e^{-\lambda\tau} H(r, n\pi/L)\right) - A = 0, \ n \in \mathbb{Z}. \tag{3.17}$$

For convenience of analysis, we set $k = n\pi/L$ in (3.17) and consider the equation

$$\lambda + d_1 k^2 + \tilde{d}_2 k^2 H(r,k) e^{-\lambda\tau} - A = 0, \ k \in \mathbb{R}, \tag{3.18}$$

where

$$H(r,k) = \begin{cases} \frac{\sin(kr)}{kr}, & k \neq 0, \\ 1, & k = 0. \end{cases} \tag{3.19}$$

*Remark* 3.2. Eq. (3.18) is the characteristic equation of the linearized equation (3.1) for the infinite interval $\Omega = (-\infty, +\infty)$ and can also be obtained by substituting $u = e^{\lambda t + ikx}$ into (3.1). If the distribution of roots of (3.18) is clear, the distribution of roots of (3.17) is also easily revealed by the relationship $k = n\pi/L$.

Throughout this paper, we always assume the condition

$$(C_1) \ \ A = f'(u_*) < 0, \ d_1 \geq -\tilde{d}_2$$

holds. The condition $A = f'(u_*) < 0$ implies that the positive equilibrium $u_*$ of the corresponding ordinary differential equation $u'(t) = f(u)$ is locally asymptotically stable. If we set $H(0,k) = 1$, then it is easy to verify that for $r = 0$ and $\tau = 0$, all roots of (3.18) are negative, provided that condition $(C_1)$ holds. This implies that the positive steady state of (1.3) is locally asymptotically stable when there is no delay (i.e., $\tau = 0$) and no nonlocal perception (i.e., $r = 0$). In what follows, we take $\tau$ and $r$ as bifurcation parameters to investigate the influence of both memory delay and nonlocal perception range on the stability of the positive steady state $u_*$ and the possible bifurcations under the basic assumption $(C_1)$.

**3.2.1. Stability and Turing bifurcation for the case of $\tau = 0$ and $r > 0$.** In this subsection, we consider the influence of the perception range $r$ on the stability of the positive steady state $u_*$ and the possible bifurcation for the case of $\tau = 0$. For fixed $k$, denote the root of (3.18) by $\lambda_k(r)$. Then when $\tau = 0$, the root of (3.18) is determined by

$$\lambda_k(r) = -d_1 k^2 - \tilde{d}_2 k^2 H(r,k) + A,$$

which, together with (3.19), implies that $\lambda_0(r) = A < 0$ and for $k \neq 0$, $\lambda_k(r) < 0$ is equivalent to

$$\tilde{d}_2 \frac{\sin(kr)}{kr} > -d_1 + \frac{A}{k^2}, \tag{3.20}$$

and $\lambda_k(r) = 0$ is equivalent to

$$H(r,k) = -\frac{d_1}{\tilde{d}_2} + \frac{A}{\tilde{d}_2 k^2}.$$

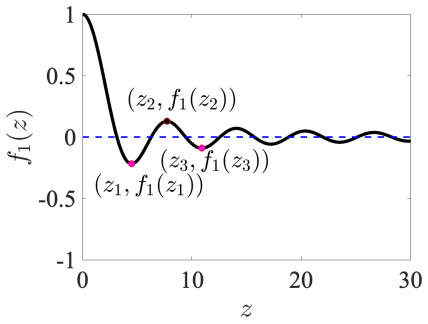


**Figure 1.** *The graph of the function $f_1(z)$ and its local extremum points.*

Letting $f_1(z) = \sin(z)/z$, it is easy to verify that

$$\frac{df_1(z)}{dz} = \frac{z\cos(z) - \sin(z)}{z^2}. \tag{3.21}$$

Denote the countable number of nonnegative roots of the equation $\tan(z) = z$ by $z_j \geq 0$ satisfying $z_0 = 0$ and $z_j < z_{j+1}, j \in \mathbb{N}_0$. Notice that $\lim_{z\to 0^+} f_1(z) = 1$. Assuming that $f_1(0) = 1$, the graph of the function $f_1(z)$ is shown in Figure 1. Then by (3.21) and Figure 1, we have the following results on the local extremum of $f_1(z)$.

Proposition 3.3. *$f_1(z)$ obtains its local extremum at $z = z_j$. More specifically, we have*

(i) *$f_1(z)$ obtains its local minimum at $z = z_j, j = 2(m-1)+1$, and*

$$f_1(z_{2m-1}) < f_1(z_{2m+1}) < 0,\ m \in \mathbb{N};$$

(ii) *$f_1(z)$ obtains its local maximum at $z = z_j, j = 2m$, and*

$$f_1(z_{2m}) > f_1(z_{2(m+1)}) > 0,\ m \in \mathbb{N}_0.$$

Letting

$$f_2^T(k) = -\frac{d_1}{\tilde{d}_2} + \frac{A}{\tilde{d}_2 k^2}, \tag{3.22}$$

it is easy to see that for fixed $r$, the curves $H = H(r,k)$ and $f_2 = f_2^T(k)$ are tangent at $k$ if and only if $(r,k)$ satisfy the following two equations:

$$H(r,k) = f_2^T(k),\ \frac{\partial H(r,k)}{\partial k} = \frac{df_2^T(k)}{dk}. \tag{3.23}$$

By Proposition 3.3, the following results follow immediately.

Proposition 3.4.

(i) *For $\tilde{d}_2 > 0$, if $-\frac{\sin(z_{2m+1})}{z_{2m+1}}\tilde{d}_2 \leq d_1 < -\frac{\sin(z_{2m-1})}{z_{2m-1}}\tilde{d}_2, m = 1,2,\ldots$, then there exist $m$ critical values $r_T^{(1)},\ldots,r_T^{(m)}$ of $r$ and $k_T^{(1)},\ldots,k_T^{(m)}$ of $k$ such that $(r,k) = (r_T^{(j)}, k_T^{(j)})$, $j = 1,\ldots,m$, satisfy (3.23).*

(ii) *For $\tilde{d}_2 < 0$, if $\frac{\sin(z_{2(m+1)})}{z_{2(m+1)}}|\tilde{d}_2| \leq d_1 < \frac{\sin(z_{2m})}{z_{2m}}|\tilde{d}_2|, m = 0,1,\ldots$, and we set $\frac{\sin(z_{2m})}{z_{2m}} = 1$ for $m = 0$, then there exist $m+1$ critical values $r_T^{(1)},\ldots,r_T^{(m+1)}$ of $r$ and $k_T^{(1)},\ldots,k_T^{(m+1)}$ of $k$ such that $(r,k) = (r_T^{(j)}, k_T^{(j)})$, $j = 1,\ldots,m+1$, satisfy (3.23).*

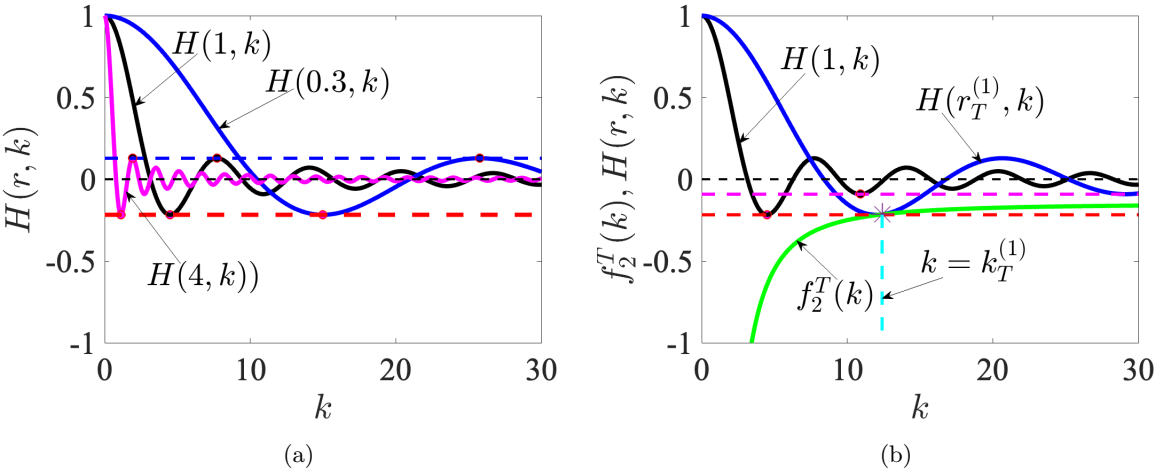


(a) (b)

**Figure 2.** (a) *The graph of* $H(r,k)$ *for different values of* $r$. (b) *The graph of* $f_2^T(k)$ *for* $d_1 = 1.5, \tilde{d}_2 = 0.1, A = -1$ *such that* $f_1(z_1) < -\frac{d_1}{\tilde{d}_2} \le f_1(z_3)$. *There exists a unique* $r = r_T^{(1)} \doteq 0.3742$ *such that* $H(r_T^{(1)}, k)$ *is tangent to the curve* $f_2^T(k)$ *at* $k = k_T^{(1)} \doteq 12.4$.

*Proof.* Notice that $z_j$ and local extremum $f_1(z_j)$ are independent of $r$. Thus the local extremum $f_1(z_j)$ (the red and blue dashed lines) of the function $H = H(r,k)$ remain constant as $r$ varies (as shown in Figure 2(a)). Setting $z_j = k_j r$, then, for fixed $z_j$, $k_j$ decreases as $r$ increases, and $\lim_{r\to+\infty} k_j = 0$. This implies that the curve $H(r,k)$ is compressed along the $k$-axis as $r$ increases; otherwise it will be stretched as $r$ decreases (as shown in Figure 2(a)).

From (3.22), $f_2^T(k)$ is independent of $r$. Thus the graph of the function $f_2 = f_2^T(k)$ is not affected by the change in $r$.

It follows from (3.22) that when $\tilde{d}_2 > 0$, the function $f_2 = f_2^T(k)$ is monotonically increasing with respect to $k$ since $A < 0$ and $\tilde{d}_2 > 0$, and $\lim_{k\to\infty} f_2^T(k) = -d_1/\tilde{d}_2 < 0$. For $-d_1/\tilde{d}_2 > f_1(z_1)$, if there exists a positive integer $m \in \mathbb{N}$ such that

$$f_1(z_{2m-1}) < -\frac{d_1}{\tilde{d}_2} \le f_1(z_{2m+1}),$$

then when $r$ is changed from large to small, the curve $H(r,k)$ is tangent to the curve $f_2 = f_2^T(k)$ for $m$ times. Figure 2(b) illustrates this fact for $m = 1$. This confirms conclusion (i) for $\tilde{d}_2 > 0$.

For $\tilde{d}_2 < 0$, the function $f_2 = f_2^T(k)$ is monotonically decreasing with respect to $k$, and $\lim_{k\to\infty} f_2^T(k) = -d_1/\tilde{d}_2 > 0$. The rest of the proof is similar to the case of $\tilde{d}_2 > 0$, so we omit it here.

By Proposition 3.4, we can prove the following results on the distribution of roots of (3.18).

Lemma 3.5. *For* $\tau = 0$ *and* $\tilde{d}_2 > 0$, *we have the following results on the roots of* (3.18):

(I) *If* $d_1 \ge -\frac{\sin z_1}{z_1}\tilde{d}_2$, *then* $\lambda_k(r) < 0$ *for any* $r \ge 0$ *and* $k \ge 0$.

(II) *If* $-\frac{\sin z_{2m+1}}{z_{2m+1}}\tilde{d}_2 \le d_1 < -\frac{\sin z_{2m-1}}{z_{2m-1}}\tilde{d}_2$, $m = 1, 2, \ldots$, *then there exists a threshold* $r_T^*$ *of* $r$ *and* $k_T^* > 0$ *such that*

(i) *for* $r > r_T^*$, $\lambda_k(r) < 0$ *for any* $k \geq 0$;
(ii) *for* $r = r_T^*$, $\lambda_{k_T^*}(r_T^*) = 0$ *and* $\lambda_k(r_T^*) < 0$ *for* $k \neq k_T^*$;
(iii) *for* $0 < r < r_T^*$, *we have*

$$\lambda_k(r) \begin{cases} < 0, & k \in I_r^-(k), \\ = 0, & k \in I_r^0(k), \\ > 0, & k \in I_r^+(k), \end{cases}$$

*where, for fixed* $r \in (0, r_T^*)$, $I_r^0(k) = \left\{k |\, H(r,k) = f_2^T(k), k \geq 0\right\}$ *and*

$$I_r^-(k) = \left\{k |\, H(r,k) > f_2^T(k), k \geq 0\right\}, I_r^+(k) = \left\{k |\, H(r,k) < f_2^T(k), k \geq 0\right\}.$$

*Proof.* It follows from (3.20) that for $\tilde{d}_2 > 0$, $\lambda_k(r) < 0$ is equivalent to

$$H(r,k) > f_2^T(k).$$

Notice that for $\tilde{d}_2 > 0$, $f_2^T(k) < 0$ since $d_1 > 0$ and $A < 0$. In addition, it is easy to verify that $f_2^T(k)$ is monotonically increasing with respect to $k$ and

$$\lim_{k \to +\infty} f_2^T(k) = -\frac{d_1}{\tilde{d}_2}, \quad \lim_{k \to 0^+} f_2^T(k) = -\infty.$$

From (i) of Proposition 3.3, we have

$$\min_{k>0, r>0} H(r,k) = \frac{\sin z_1}{z_1}.$$

Thus, for $d_2 > 0$, $\lambda_k(r) < 0$, provided that $-\frac{d_1}{\tilde{d}_2} \leq \frac{\sin z_1}{z_1}$. This completes the proof of (I).

In what follows, we first prove conclusion (II) for $m = 1$. Notice that $-\frac{\sin z_3}{z_3}\tilde{d}_2 \leq d_1 < -\frac{\sin z_1}{z_1}\tilde{d}_2$ is equivalent to

$$\frac{\sin z_1}{z_1} < -\frac{d_1}{\tilde{d}_2} \leq \frac{\sin z_3}{z_3}$$

and $\lim_{r \to +\infty} z_1/r = 0$. Therefore, when $r$ is large enough, we have

$$H(r,k) > f_2^T(k), \ k \geq 0.$$

With the decreasing of $r$ and $r > r_T^{(1)}$, we still have $H(r,k) > f_2^T(k)$. This implies that $\lambda_k(r) < 0$ for $r > r_T^{(1)}$ and any $k \geq 0$. In terms of (i) of Proposition 3.4, when $r = r_T^{(1)}$, the curves $H = H\left(r_T^{(1)}, k\right)$ and $f_2 = f_2^T(k)$ are tangent at $k = k_T^{(1)}$. When $0 < r < r_T^{(1)}$, the curves $H = H(r,k)$ and $f_2 = f_2^T(k)$ intersect at $k = k_c^{(1)}$ and $k = k_c^{(2)}$, and

$$\begin{cases} H(r,k) > f_2^T(k), & k \in \left[0, k_c^{(1)}\right) \cup \left(k_c^{(2)}, +\infty\right), \\ H(r,k) = f_2^T(k), & k = k_c^{(1)}, k_c^{(2)}, \\ H(r,k) < f_2^T(k), & k \in \left(k_c^{(1)}, k_c^{(2)}\right). \end{cases}$$

Letting $r_T^* = r_T^{(1)}$ and $k_T^* = k_T^{(1)}$ and

$$I_r^0(k) = \left\{k_c^{(1)}, k_c^{(2)}\right\},\ I_r^-(k) = \left[0, k_c^{(1)}\right) \cup \left(k_c^{(2)}, +\infty\right),\ I_r^+(k) = \left(k_c^{(1)}, k_c^{(2)}\right),$$

the proof of (II) is complete for $m = 1$. For $m = 2, 3, \ldots$, letting

$$r_T^* = \max\left\{r_T^{(1)}, \ldots, r_T^{(m)}\right\} = r_T^{(j)},\ j \in \{1, \ldots, m\}, \tag{3.24}$$

and $k_T^* = k_T^{(j)}$, similar to the proof for $m = 1$, it is easy to confirm (II). ∎

For $d_2 < 0$, it follows from (3.20) that $\lambda_k(r) < 0$ is equivalent to $H(r,k) < f_2^T(k)$. Then, employing (ii) of Propositions 3.3 and 3.4 and using a proof similar to that for $d_2 > 0$, we can similarly prove the following lemma for $d_2 < 0$.

Lemma 3.6. *For $\tau = 0$ and $\tilde{d}_2 < 0$, we have the following results on the roots of (3.18):*

(I) *If $d_1 \geq \left|\tilde{d}_2\right|$, then $\lambda_k(r) < 0$ for any $r \geq 0$ and $k \geq 0$.*

(II) *If $\frac{\sin z_{2(m+1)}}{z_{2(m+1)}}\left|\tilde{d}_2\right| \leq d_1 < \frac{\sin z_{2m}}{z_{2m}}|\tilde{d}_2|, m = 0, 1, \ldots$, then there exists a threshold $r_T^*$ of $r$ and $k_T^* > 0$ such that*

(i) *for $r > r_T^*$, $\lambda_k(r) < 0$ for any $k \geq 0$;*

(ii) *for $r = r_T^*$, $\lambda_{k_T^*}(r_T^*) = 0$ and $\lambda_k(r_T^*) < 0$ for $k \neq k_T^*$;*

(iii) *for $0 < r < r_T^*$, we have*

$$\lambda_k(r) \begin{cases} < 0, & k \in I_r^+(k), \\ = 0, & k \in I_r^0(k), \\ > 0, & k \in I_r^-(k). \end{cases}$$

From Lemma 3.5 and noticing that the condition $d_1 \geq -\tilde{d}_2$ in condition $(C_1)$ naturally holds for $d_2 > 0$, we have the following theorem.

Theorem 3.7. *Assume that $d_2 > 0$ and $f'(u_*) < 0$. When $\tau = 0$, we have the following results on the stability and bifurcation of the positive steady state $u_*$ of (1.3):*

(I) *If $d_1 \geq -\frac{\sin z_1}{z_1}\tilde{d}_2$, then $u_*$ is asymptotically stable for any $r > 0$.*

(II) *If $d_1 < -\frac{\sin z_1}{z_1}\tilde{d}_2$, then there exists a threshold $r_T^*$ of $r$ such that*

(i) *for $r > r_T^*$, $u_*$ is asymptotically stable;*

(ii) *for $0 < r < r_T^*$, $u_*$ is unstable;*

(iii) *(1.3) undergoes Turing bifurcation at $r = r_T^*$.*

*Remark* 3.8. If there exist multiple $j_1, j_2, \ldots, j_N \in \{1, \ldots, m\}$ in (3.24) such that $r_T^* = r_T^{(j_k)}$, then $\lambda_{k_T^{(j_k)}}\left(r_T^{(j_k)}\right) = 0, k = 1, \ldots, N$. In this case, (1.3) may undergo multiple Turing bifurcations at $r = r_T^*$. However, for $-\frac{\sin z_3}{z_3}\tilde{d}_2 \leq d_1 < -\frac{\sin z_1}{z_1}\tilde{d}_2$, we have $r_T^* = r_T^{(1)}$ and $k_T^* = k_T^{(1)}$, and thus (1.3) undergoes single Turing bifurcation at $r = r_T^*$.

Notice that when condition $(C_1)$ holds, we have $d_1 \geq -\tilde{d}_2$. From Lemma 3.6(I), all roots of the characteristic equation (3.18) are negative for all $r > 0$ and $k \in \mathbb{R}$. Then we have the following theorem.

Theorem 3.9. *Assume that $d_2 < 0$ and condition $(C_1)$ holds. When $\tau = 0$, the positive steady state $u_*$ of (1.3) is asymptotically stable for any $r > 0$.*

**3.2.2. Hopf bifurcation and Turing–Hopf bifurcation for the case of $\tau > 0$ and $r > 0$.** In the following, under the assumption that $u_*$ is asymptotically stable for $\tau = 0$, we further investigate the distribution of the purely imaginary roots of (3.18) for $\tau > 0$. Letting $\lambda = \eta + i\omega(\omega > 0)$ be the root of (3.18), substituting it into (3.18), and then separating the real and imaginary parts, we have

$$\begin{cases} \eta + d_1k^2 + \tilde{d}_2k^2H(r,k)e^{-\eta\tau}\cos(\omega\tau) - A = 0, \\ \omega - \tilde{d}_2k^2H(r,k)e^{-\eta\tau}\sin(\omega\tau) = 0. \end{cases} \tag{3.25}$$

From the first equation of (3.25), we have

$$\eta e^{\eta\tau} + \left(d_1k^2 - A\right)e^{\eta\tau} = -\tilde{d}_2k^2H(r,k)\cos(\omega\tau).$$

Notice that $\lim_{r\to+\infty} H(r,k) = 0$. Thus, if $\eta \geq 0$, we get a contradiction since $\eta e^{\eta\tau} + \left(d_1k^2 - A\right)e^{\eta\tau} \geq d_1k^2 - A > 0$. Therefore, we can deduce that for any fixed $k \in \mathbb{R}$ and $\tau > 0$, all roots of (3.18) have negative real parts, provided that $r$ is large enough. In the following, we investigate whether or not (3.18) has purely imaginary roots when $r$ is decreasing.

Substituting $\eta = 0$ into (3.25), we have

$$\begin{cases} \tilde{d}_2k^2H(r,k)\cos(\omega\tau) = A - d_1k^2, \\ \tilde{d}_2k^2H(r,k)\sin(\omega\tau) = \omega, \end{cases} \tag{3.26}$$

which yields to

$$\omega^2 = \left(\tilde{d}_2k^2H(r,k) + d_1k^2 - A\right)\left(\tilde{d}_2k^2H(r,k) - d_1k^2 + A\right). \tag{3.27}$$

Assume that there exists $\omega_k > 0$ defined by

$$\omega_k = \sqrt{\left(\tilde{d}_2k^2H(r,k) + d_1k^2 - A\right)\left(\tilde{d}_2k^2H(r,k) - d_1k^2 + A\right)} \tag{3.28}$$

such that (3.27) holds. Then we can solve (3.26) for $\tau$. It follows from the second equation of (3.26) that $\sin(\omega\tau) > 0$ for $\tilde{d}_2H(r,k) > 0$ and $\sin(\omega\tau) < 0$ for $\tilde{d}_2H(r,k) < 0$, which implies that $\omega\tau$ is in the first and second quadrants for $\tilde{d}_2H(r,k) > 0$ and $\omega\tau$ is in the third and fourth quadrants for $\tilde{d}_2H(r,k) < 0$. Thus, if we define

$$\tau_{k,j} = \begin{cases} \frac{1}{\omega_k}\left\{\arccos\frac{A-d_1k^2}{\tilde{d}_2k^2H(r,k)} + 2j\pi\right\}, & \tilde{d}_2H(r,k) > 0, \\ \frac{1}{\omega_k}\left\{2\pi - \arccos\frac{A-d_1k^2}{\tilde{d}_2k^2H(r,k)} + 2j\pi\right\}, & \tilde{d}_2H(r,k) < 0, \end{cases} \tag{3.29}$$

then (3.18) has a pair of purely imaginary roots $\pm i\omega_k$ at $\tau = \tau_{k,j}, j \in \mathbb{N}_0$.

Setting

$$f_2^H(k) = \frac{d_1}{\tilde{d}_2} - \frac{A}{\tilde{d}_2k^2}, \tag{3.30}$$

by (3.28) it is easy to verify the following results on the existence of $\omega_k > 0$.

Proposition 3.10. *Assume that $f_2^T(k)$ and $f_2^H(k)$ are defined by (3.22) and (3.30), respectively.*

(i) *For $\tilde{d}_2 > 0$, $\omega_k > 0$ if and only if there are $r$ and $k$ such that either $H(r,k) > f_2^H(k)$ or $H(r,k) < f_2^T(k)$ holds.*

(ii) *For $\tilde{d}_2 < 0$, $\omega_k > 0$ if and only if there are $r$ and $k$ such that either $H(r,k) < f_2^H(k)$ or $H(r,k) > f_2^T(k)$ holds.*

Taking $\tau$ as the bifurcation parameter and letting $\lambda = \lambda(\tau)$ be the root of (3.18) satisfying $\mathrm{Re}\lambda(\tau_{k,j}) = 0$ and $\mathrm{Im}\lambda(\tau_{k,j}) = \omega_k$, it follows from (3.18) that

$$\frac{d\lambda(\tau)}{d\tau} = \frac{\lambda \tilde{d}_2 k^2 H(r,k) e^{-\lambda\tau}}{1 - \tau \tilde{d}_2 k^2 H(r,k) e^{-\lambda\tau}}. \tag{3.31}$$

By (3.18) and (3.31), we have

$$\left(\frac{d\lambda(\tau)}{d\tau}\right)^{-1} = \frac{1}{\lambda(-\lambda - d_1 k^2 + A)} - \frac{\tau}{\lambda}.$$

Noticing that $\mathrm{Re}\lambda(\tau_{k,j}) = 0$ and $\mathrm{Im}\lambda(\tau_{k,j}) = \omega_k$, we have

$$\mathrm{Re}\left(\left(\frac{d\lambda(\tau)}{d\tau}\right)^{-1}\Big|_{\tau=\tau_{k,j}}\right) = \frac{1}{\omega_k^2 + (A - d_1 k^2)^2} > 0.$$

In addition, according to the fact that $d\mathrm{Re}\lambda(\tau)/d\tau = \mathrm{Re}(d\lambda(\tau)/d\tau)$ and the signs of $\mathrm{Re}(d\lambda(\tau)/d\tau)$ and $\mathrm{Re}((d\lambda(\tau)/d\tau)^{-1})$ are the same, we have the following transversality condition for Hopf bifurcation:

$$\frac{d\mathrm{Re}\lambda(\tau_{k,j})}{d\tau} > 0. \tag{3.32}$$

Similarly, taking $r$ as the bifurcation parameter and letting $\lambda = \lambda(r)$ be the real root of (3.18) with $k = k_T^*$ satisfying $\lambda(r_T^*) = 0$, from (3.18) we have

$$\frac{d\lambda(r)}{dr} = \frac{-\tilde{d}_2 k^2 H_r(r,k) e^{-\lambda\tau}}{1 - \tau \tilde{d}_2 k^2 H(r,k) e^{-\lambda\tau}}, \tag{3.33}$$

where the partial derivative $H_r(r,k)$ of $H(r,k)$ with respect to $r$ is

$$H_r(r,k) = \frac{\cos(kr)(kr - \tan(kr))}{kr^2}.$$

This, together with the fact that $\lambda = 0$ is a root of (3.18) for $k = k_T^*, r = r_T^*$, and $\pi < z_1 < k_T^* r_T^* < \frac{3\pi}{2}$, implies that $H_r(r_T^*, k_T^*) > 0$. Thus, by (3.33), we have

$$\frac{d\lambda(r)}{dr}\Big|_{r=r_T^*, k=k_T^*} = \frac{-\tilde{d}_2 (k_T^*)^2 H_r(r_T^*, k_T^*)}{1 + \tau d_1 (k_T^*)^2 - \tau A} = \begin{cases} < 0, & \tilde{d}_2 > 0, \\ > 0, & \tilde{d}_2 < 0. \end{cases} \tag{3.34}$$

By Lemmas 3.5 and 3.6, Proposition 3.10, and (3.32) and (3.34), we can prove the following theorem on the stability of $u_*$ and bifurcation due to the joint effect of the perception range $r$ and memory delay $\tau$.

Theorem 3.11. *Assume that $d_2>0$ and $f'(u_*)<0$. We have the following results:*

1. *If $d_1\geq \tilde{d}_2$, then $u_*$ is asymptotically stable for any $r\geq 0$ and $\tau\geq 0$.*
2. *If $|\frac{\sin z_1}{z_1}\tilde{d}_2|\leq d_1<\tilde{d}_2$, then there exists a threshold $r_H^*$ of $r$ such that*
   (i) *when $r\geq r_H^*$, $u_*$ is asymptotically stable for any $\tau\geq 0$;*
   (ii) *when $0<r<r_H^*$, there exists a critical value $\tau_*$ such that $u_*$ is asymptotically stable for $0\leq\tau<\tau_*$ and unstable for $\tau>\tau_*$, and (1.3) undergoes Hopf bifurcation at $\tau=\tau_*$.*
3. *If $|\frac{\sin z_{j+1}}{z_{j+1}}\tilde{d}_2|\leq d_1<|\frac{\sin z_j}{z_j}\tilde{d}_2|$, $j\in\mathbb{N}$, then we have the following results:*
   (1) *When $r_T^*\geq r_H^*$, $u_*$ is asymptotically stable for $r>r_T^*$ and any $\tau\geq 0$ and unstable for $0<r<r_T^*$ and any $\tau\geq 0$, and (1.3) undergoes Turing bifurcation at $r=r_T^*$.*
   (2) *When $r_T^*<r_H^*$, delay-induced Hopf bifurcations and Turing–Hopf bifurcation appear. More specifically,*
      (i) *for $r\geq r_H^*$, $u_*$ is asymptotically stable for any $\tau\geq 0$;*
      (ii) *for $r_T^*<r<r_H^*$, there exists a critical value $\tau_*$ such that $u_*$ is asymptotically stable for $0\leq\tau<\tau_*$ and unstable for $\tau>\tau_*$, and (1.3) undergoes Hopf bifurcation at $\tau=\tau_*$;*
      (iii) *for $r<r_T^*$, $u_*$ is unstable stable for any $\tau\geq 0$;*
      (iv) *(1.3) undergoes Turing–Hopf bifurcation at $(r,\tau)=(r_T^*,\tau_*)$.*

*Proof.* In what follows, keep in mind the fact that if $\lambda=0$ is a root of (3.18) for $\tau=0$, then it is still a root of (3.18) for $\tau>0$.

1. For $d_1\geq\tilde{d}_2$, it follows from Lemma 3.5 that for $\tau=0$, all roots of (3.18) are negative since $d_1\geq\tilde{d}_2>-\frac{\sin z_1}{z_1}\tilde{d}_2$, and it is easy to verify that for any $r>0,k>0$,
$$H(r,k)\leq 1\leq\frac{d_1}{\tilde{d}_2}<f_2^H(k)$$
and
$$f_2^T(k)<-\frac{d_1}{\tilde{d}_2}\leq -1<H(r,k).$$
This, together with (i) of Proposition 3.10, implies that for $\tau>0$, (3.18) has no purely imaginary roots for $d_1\geq\tilde{d}_2$. Therefore, all roots of (3.18) have negative real parts for $d_1\geq\tilde{d}_2$. This completes the proof for $d_2>0$.
2. For $-\frac{\sin z_1}{z_1}\tilde{d}_2\leq d_1<\tilde{d}_2$ and $\tau=0$, all roots of (3.18) are negative from Lemma 3.5. In this case, it is easy to verify that for any $r>0,k>0$,
$$f_2^T(k)<-\frac{d_1}{\tilde{d}_2}\leq\frac{\sin z_1}{z_1}<H(r,k).$$
For $\tilde{d}_2>0$, it is easy to verify that $f_2^H(k)$ is monotonically decreasing with respect to $k$ and
$$\lim_{k\to+\infty}f_2^H(k)=\frac{d_1}{\tilde{d}_2}>0,\ \lim_{k\to 0^+}f_2^H(k)=+\infty.$$
Notice that
$$\frac{d_1}{\tilde{d}_2}<1,\ \lim_{z\to 0}\frac{\sin z}{z}=1,\ \lim_{z\to+\infty}\frac{\sin z}{z}=0,\ z=rk,$$

and $f_2^H(k)$ is independent of $r$. Thus, we can conclude that there exists a threshold $r_H^*$ such that

(i) for $r > r_H^*$, $H(r,k) < f_2^H(k)$ for any $k > 0$;
(ii) for $r = r_H^*$, the curves $H = H(r_H^*, k)$ and $f_2 = f_2^H(k)$ are tangent at $k = k_H^*$;
(iii) for $0 < r < r_H^*$, there exist two values $k_c^{(1)}, k_c^{(2)} > 0$ such that the curves $H = H(r,k)$ and $f_2 = f_2^H(k)$ intersect at $k = k_c^{(1)}$ and $k = k_c^{(2)}$, and $H(r,k) > f_2^H(k)$ for $k \in (k_c^{(1)}, k_c^{(2)})$ and $H(r,k) < f_2^H(k)$ for $k \in (0, k_c^{(1)}) \cup (k_c^{(2)}, +\infty)$.

This, together with (i) of Proposition 3.10, implies that when $0 < r < r_H^*$, $\omega_k$ exists for any fixed $k \in (k_c^{(1)}, k_c^{(2)})$. Furthermore, by the transversality condition (3.32) and Lemma 3.5, we have the following results:

(i) When $r \geq r_H^*$, all roots of (3.18) have negative real parts for any $\tau \geq 0$.
(ii) When $0 < r < r_H^*$, there exists a critical value $\tau_*$ such that all roots of (3.18) have negative real parts for $0 \leq \tau < \tau_*$ and (3.18) has a pair of purely imaginary roots $\pm i\omega_k$ at $\tau = \tau_*$, where

$$\tau_* = \min_{k \in (k_c^{(1)}, k_c^{(2)})} \{\tau_{k,0}\}.$$

This, together with transversality condition (3.32), complete the proof for $\tilde{d}_2 > 0$.

3. We first prove this conclusion for $j = 1$, i.e.,

$$\frac{\sin z_2}{z_2}\tilde{d}_2 \leq d_1 < -\frac{\sin z_1}{z_1}\tilde{d}_2.$$

For this case, we have

$$\frac{\sin z_2}{z_2} \leq \frac{d_1}{\tilde{d}_2} < 1, \; -1 < \frac{\sin z_1}{z_1} < -\frac{d_1}{\tilde{d}_2} \leq \frac{\sin z_3}{z_3}.$$

Then, by the properties of the functions $f_2 = f_2^T(k)$, $f_2 = f_2^H(k)$, and $H = H(r,k)$, we can conclude that there exist critical values $r_H^{(1)}$ and $r_T^{(1)}$ such that $H = H(r_H^{(1)}, k)$ and $f_2 = f_2^H(k)$ are tangent at $k = k_H^{(1)}$, and $H = H(r_T^{(1)}, k)$ and $f_2 = f_2^T(k)$ are tangent at $k = k_T^{(1)}$, and for $r > \max\{r_T^{(1)}, r_H^{(1)}\}$, we have $f_2^T(k) < H(r,k) < f_2^H(k)$, which, together with (i) of Proposition 3.10, implies that (3.18) has no purely imaginary roots for $\tau > 0$. Furthermore, the discussion is divided into two cases according to whether $r_T^{(1)}$ is larger than $r_H^{(1)}$ or not.

(1) For $r_T^{(1)} \geq r_H^{(1)}$,
  (i) when $r > r_T^{(1)}$, all roots of (3.18) have negative real parts for any $\tau \geq 0$;
  (ii) when $r = r_T^{(1)}$, we have $\lambda_{k_T^{(1)}}(r_T^{(1)}) = 0$, and $\lambda_k(r_T^{(1)}) < 0$ for $k \neq k_T^{(1)}$. And (3.18) has at least one positive root for $0 < r < r_T^{(1)}$ and $\tau \geq 0$ under the transversality condition (3.34).
(2) For $r_T^{(1)} < r_H^{(1)}$,
  (i) when $r \geq r_H^{(1)}$, all roots of (3.18) have negative real parts for any $\tau \geq 0$;
  (ii) when $0 < r < r_H^{(1)}$, there exist two values $k_c^{(1)}, k_c^{(2)} > 0$ such that the curves $H = H(r,k)$ and $f_2 = f_2^H(k)$ intersect at $k = k_c^{(1)}$ and $k = k_c^{(2)}$, and $H(r,k) > f_2^H(k)$ for $k \in (k_c^{(1)}, k_c^{(2)})$ and $H(r,k) < f_2^H(k)$ for $k \in (0, k_c^{(1)}) \cup (k_c^{(2)}, +\infty)$. This, together

with (i) of Proposition 3.10, implies that $\omega_k$ exists for any fixed $k \in (k_c^{(1)}, k_c^{(2)})$ and (3.18) has a pair of purely imaginary roots $\pm i\omega_k$ at $\tau = \tau_{k,j}$;

(iii) when $r = r_T^{(1)} < r_H^{(1)}$, $\lambda_{k_T^{(1)}}(r_T^{(1)}) = 0$ for any $\tau \geq 0$. This, together with (ii) in this case, implies that for $(r, \tau) = (r_T^*, \tau_{k,j})$, (3.18) has a pair of purely imaginary roots $\pm i\omega_k$ and a zero root and all other roots have negative real parts.

Then, letting $r_T^* = r_T^{(1)}, r_H^* = r_H^{(1)}$, $\tau_* = \min_{k \in (k_c^{(1)}, k_c^{(2)})} \{\tau_{k,0}\}$, by Lemma 3.5 and transversality conditions (3.32) and (3.34), the conclusion is confirmed for $j = 1$.

For $j \in \mathbb{N}$ and $j > 1$, assume that there exist $(r, k) = (r_H^{(j)}, k_H^{(j)})$, $j = 1, \ldots, j_1$, satisfying

$$H(r,k) = f_2^H(k), \quad \frac{\partial H(r,k)}{\partial k} = \frac{df_2^H(k)}{dk}, \tag{3.35}$$

and there exist $(r, k) = (r_T^{(j)}, k_T^{(j)})$, $j = 1, \ldots, j_2$, satisfying (3.23).

Letting

$$r_T^* = \max\left\{r_T^{(1)}, \ldots, r_T^{(j_1)}\right\}, \quad r_H^* = \max\left\{r_H^{(1)}, \ldots, r_H^{(j_2)}\right\},$$

then the rest of the proof is very similar to the case of $j = 1$, and we omit it here. ∎

*Remark* 3.12. For case (1) of result 3 in Theorem (3.11), when $r < r_T^*$, the positive real root of the corresponding characteristic equation always exists. Therefore, when $r < r_T^*$, the positive constant steady state $u_*$ is always unstable for any $\tau > 0$. For $r_H^* < r < r_T^*$ or $0 < r < r_H^*$, delay-induced Hopf bifurcation is possible, which occurs after $u_*$ loses its stability. Here we only focus on the stability of $u_*$ and the bifurcation occurring at the stability boundaries.

For $d_2 < 0$, it follows from (3.22) and (3.30) that $f_2^H(k)$ is monotonically increasing with respect to $k$ and

$$\lim_{k \to +\infty} f_2^H(k) = \frac{d_1}{\tilde{d}_2} < 0, \quad \lim_{k \to 0^+} f_2^H(k) = -\infty, \tag{3.36}$$

and $f_2^T(k)$ is monotonically decreasing with respect to $k$ and

$$\lim_{k \to +\infty} f_2^T(k) = -\frac{d_1}{\tilde{d}_2} > 0, \quad \lim_{k \to 0^+} f_2^T(k) = +\infty. \tag{3.37}$$

Notice that if condition $(C_1)$ holds, we have

$$\frac{d_1}{\tilde{d}_2} \leq -1, \quad -\frac{d_1}{\tilde{d}_2} \geq 1,$$

which, together with (3.36) and (3.37), implies that for any $r > 0$ and $k > 0$,

$$f_2^H(k) < H(r,k) < f_2^T(k). \tag{3.38}$$

From Proposition (3.10) and (3.38), the following theorem is easily confirmed.

Theorem 3.13. *Assume that $d_2 < 0$ and condition $(C_1)$ holds. Then when $\tau > 0$, the positive constant steady state $u_*$ of (1.3) is asymptotically stable for any $r > 0$.*

*Remark* 3.14. Although the theoretical results shown in section 3.2 are proved for the infinite interval $\Omega = (-\infty, +\infty)$, it is still applicable for the finite interval $\Omega = (-L, L)$ with periodic boundary condition by choosing $n$ such that $n\pi/L$ satisfies the requirements for $k$ as shown in subsection 3.2.

**4. Application to the logistic growth model.** In this section, we employ the MATLAB software to illustrate the influence of the perceptual scale $r$ and memory delay $\tau$ on the stability of the positive constant steady state $u_*$ and pattern formation for $d_2 > 0$. For this purpose, we choose the reaction term $f(u) = gu(1-u)$ (logistic growth) and consider the following problem:

$$\begin{cases} \frac{\partial u}{\partial t} = d_1 \frac{\partial^2 u}{\partial x^2} + d_2 \frac{\partial}{\partial x}\left(u \frac{\partial}{\partial x}(K_r * u_\tau\right) + gu(1-u), -L < x < L, \\ u(-L,t) = u(L,t), \quad u_x(-L,t) = u_x(L,t) = 0, \end{cases} \tag{4.1}$$

where $g$ is the per-capita growth rate and we choose $g = 0.8$ for the following analysis and numerical simulations. Equation (4.1) has the positive constant steady state $u_* = 1$ and $\tilde{d}_2 = d_2 u_* = d_2$.

Notice that for the periodic boundary problem (4.1), the results in subsection 3.2 are satisfied by setting $k = n\pi/L$ and we denote the Hopf bifurcation values $\tau_{k,j}$ by $\tau_{n,j}$ with $n \in \mathbb{N}_0$. In addition, in order for $K_r * u_\tau$ as defined by (1.4) to have reasonable definition for any $x \in (-L, L)$, the supplement condition (1.6) is used in the numerical calculation and numerical simulations.

By the definition $z_j$ in Proposition 3.3, we have

$$\frac{\sin z_1}{z_1} \doteq -0.2172 < 0, \ \frac{\sin z_2}{z_2} \doteq 0.1283 > 0, \ \frac{\sin z_3}{z_3} \doteq -0.0913 < 0, \ \frac{\sin z_4}{z_4} \doteq 0.0709 > 0,$$

which will be used in the following numerical analysis.

**4.1. For $|\frac{\sin z_1}{z_1}|\tilde{d}_2 < d_1 < \tilde{d}_2$: memory-delay-induced Hopf bifurcation.** In this subsection, we choose $d_1 = 0.4, d_2 = 1$ such that $|\frac{\sin z_1}{z_1}|\tilde{d}_2 < d_1 < \tilde{d}_2$. Then, when $\tau = 0$, it follows from Theorem 3.7 that the positive constant steady state $u_* = 1$ is asymptotically stable for any $r \geq 0$. By (3.22) and (3.30), we have

$$f_2^T(k) = -\frac{4}{5k^2} - \frac{2}{5}, \ f_2^H(k) = \frac{4}{5k^2} + \frac{2}{5}.$$

When $\tau > 0$, there exists a threshold $r_H^*$ such that the curves $h = H(r_H^*, k)$ and $f_2 = f_2^H(k)$ are tangent at $k = k_H^*$ and $f_2^T(k) < H(r,k)$ for any $r > 0$ and $k > 0$, as shown in Figure 3(a), where $r_H^*$ can be calculated by the following procedure.

From $f_2^H(k) = H(r,k)$, we have

$$\frac{4}{5k^2} + \frac{2}{5} = \frac{\sin(z)}{z}, \tag{4.2}$$

where $z = kr > 0$. From (4.2), we have

$$\frac{\sin(z)}{z} - \frac{2}{5} > 0, \tag{4.3}$$

which implies $0 < z < 1.982$. From $\frac{df_2^H(k)}{dk} = \frac{\partial H(r,k)}{\partial k}$, we have

$$-\frac{8}{5k^3} = \frac{r(z\cos(z) - \sin(z))}{z^2}. \tag{4.4}$$

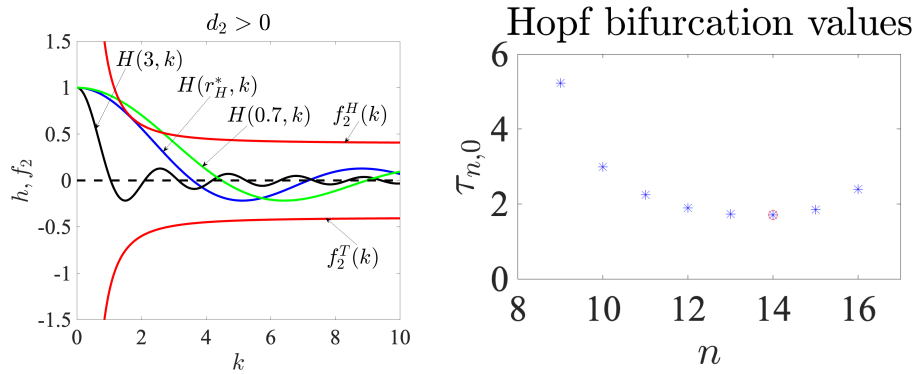


(a) (b)

**Figure 3.** (a) *For* $d_1 = 0.4, d_2 = 1$ *such that* $|\frac{\sin z_1}{z_1}|\tilde{d}_2 < d_1 < \tilde{d}_2$, *the bifurcation curves* $h = H(r,k), f_2 = f_2^T(k), f_2 = f_2^H(k)$. *The curves* $h = H(r,k)$ *and* $f_2 = f_2^H(k)$ *are tangent at* $r = r_H^* \doteq 0.8649, k = k_H^* \doteq 1.6808$. (b) *For fixed* $r = 0.7$, *the critical values* $\tau_{n,0}$ *of delay-induced Hopf bifurcations and* $\tau_* = \tau_{14,0}$.

Removing $k$ by (4.2) and (4.4), we have

$$\frac{\sin(z)}{z} + \cos(z) = \frac{4}{5}. \tag{4.5}$$

Solving (4.5) for $0 < z < 1.982$, we have $z_* \doteq 1.4537$ and then, substituting it into (4.2), we obtain the critical value $k_H^* \doteq 1.6808$. We then have

$$r_H^* = \frac{z_*}{k_H^*} \doteq 0.8649.$$

From Theorem 3.11, when $r < r_H^* \doteq 0.8649$, there exist delay-induced Hopf bifurcations for (4.1). For fixed $r = 0.7 < r_H^* \doteq 0.8649$, the curves $h = H(0.7,k)$ and $f_2 = f_2^H(k)$ intersect at $k = k_1, k_2$, where $k_1 \doteq 1.3110$ and $k_2 \doteq 2.664$.

In the rest of this subsection, we take $L = 20$ for numerical analysis and simulations. For $L = 20$ and by $k_1 < n\pi/L < k_2$, we have $n = 9, 10, \ldots, 16$, and the corresponding Hopf bifurcation values $\tau_{n,0}$ are plotted in Figure 3(b). From Figure 3(b), we have

$$\tau_* = \min_{n\in\{9,10,\ldots,16\}} \{\tau_{n,0}\} = \tau_{14,0} \doteq 1.7023.$$

Thus, the positive constant steady state $u_*$ is asymptotically stable for $\tau < \tau_*$, as shown in Figure 4(a) for $\tau = 1.5 < \tau_*$, and unstable for $\tau > \tau_*$. $\tau = \tau_*$ is the first delay-induced Hopf bifurcation value for (4.1). For $\tau = 1.72$ being larger than and close to the first Hopf bifurcation value $\tau_*$, Figure 4(b) illustrates the delay-induced periodic spot patterns. For $\tau = 8$ far from the first Hopf bifurcation value $\tau_*$, Figure 4(c) shows the existence of ladder-shaped periodic patterns.

**4.2. For $|\frac{\sin z_2}{z_2}\tilde{d}_2| \le d_1 < |\frac{\sin z_1}{z_1}\tilde{d}_2|$: perceptual-scale-induced Turing bifurcation, memory-delay-induced Hopf bifurcation, and their interaction.** Choosing $d_1 = 0.2, d_2 = 1$ such that $|\frac{\sin z_2}{z_2}\tilde{d}_2| \le d_1 < |\frac{\sin z_1}{z_1}\tilde{d}_2|$, by (3.22) we then have

$$f_2^T(k) = -\frac{4}{5k^2} - \frac{1}{5}.$$

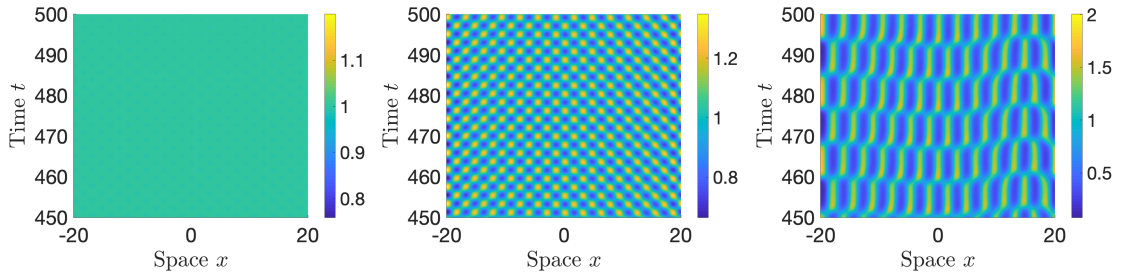


**Figure 4.** *For $d_1 = 0.4, d_2 = 1$, and $r = 0.7 < r_H^*$, delay-induced periodic patterns of (4.1) for different delays.* (a) $\tau = 1.5$. (b) $\tau = 1.72$. (c) $\tau = 8$. *The initial function is $u(x,t) = u_* + 0.2\cos(2x)$ for $t \in [-\tau, 0]$.*

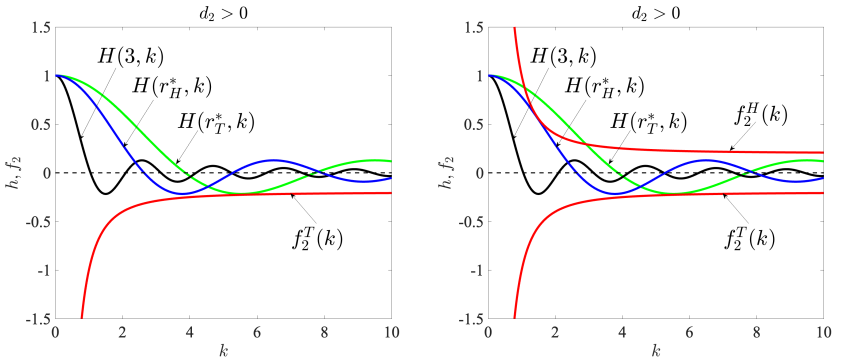


**Figure 5.** *For $d_1 = 0.2$ and $d_2 = 1 > 0$ such that $|\frac{\sin z_2}{z_2}\tilde{d}_2| \le d_1 < |\frac{\sin z_1}{z_1}\tilde{d}_2|$, the bifurcation curves $h = H(r,k), f_2 = f_2^T(k), f_2 = f_2^H(k)$.* (a) *For $\tau = 0$, the curves $h = H(r_T^*,k)$ and $f_2 = f_2^T(k)$ are tangent and Turing bifurcation occurs for (4.1), where $r_T^* \doteq 0.8128$.* (b) *For $\tau > 0$, the curves $H = H(r_T^*,k)$ and $f_2 = f_2^T(k)$ are tangent and the curves $H = H(r_H^*,k)$ and $f_2 = f_2^H(k)$ are tangent, where $r_T^* \doteq 0.8128, r_H^* \doteq 1.1896$, and there exist delay-induced Hopf bifurcations for $r_T^* < r < r_H^*$ and Turing-Hopf bifurcation for (4.1) at $r = r_T^*$ and $\tau = \tau_*$.*

The curve $f_2 = f_2^T(k)$ is tangent to the curve $h = H(r_T^*,k)$ with $r_T^* \doteq 0.8128$ at $k = k_T^* \doteq 5.5612$ as shown in Figure 5(a) for $\tau = 0$ and Figure 5(b) for $\tau > 0$. And when $r > r_T^* \doteq 0.8128$, $H(r,k) > f_2^T(k)$ for any $k \ge 0$. The calculation of $r_T^*$ is very similar to that of $r_H^*$, and we omit it here.

In what follows, we numerically illustrate the patterns induced by perceptual scale $r$ and memory delay $\tau$.

**4.2.1. Perceptual-scale-induced Turing bifurcation.** We first consider the case of $\tau = 0$. Noticing the periodic boundary condition and $r = r_T^* \doteq 0.8128$, we should choose $L$ such that there exists an $n \in \mathbb{N}$ satisfying $\frac{n\pi}{L} = k_T^*$. For this purpose, we choose $n = 18$ and $L = n\pi/k_T^* \doteq 10$, which is used in the following numerical calculations and simulations. From Theorem 3.7, (4.1) undergoes mode-18 Turing bifurcation at $r = r_T^* \doteq 0.8128$ when $\tau = 0$.

For $r = 0.9 > r_T^*$, Figure 6(a) shows the stability of the positive constant steady state $u_* = 1$. When $r$ is decreasing across the Turing bifurcation value $r_T^*$, the nonconstant steady state (vertical stripe pattern) appears as shown in Figure 6(b) for $r = 0.8$ smaller than and

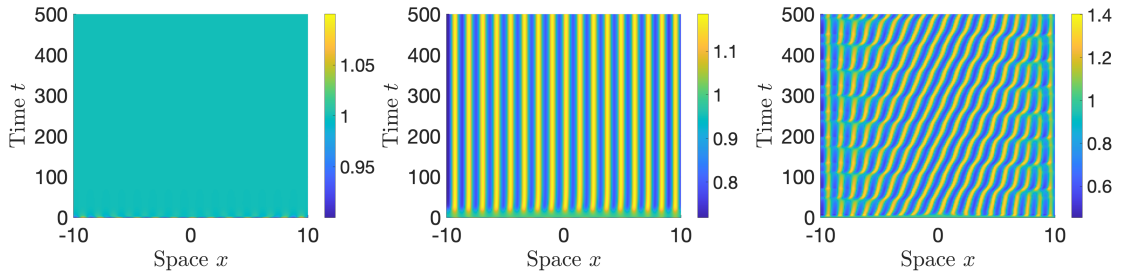


**Figure 6.** *For $d_1 = 0.2, d_2 = 1$, and $\tau = 0$, the dynamical evolution of the solutions of (4.1) with the decreasing of $r$. (a) $r = 0.9 > r_T^*$. (b) $r = 0.8 < r_T^*$. (c) $r = 0.68 < r_T^*$. The initial function is chosen as $u(x,0) = u_* + 0.1\cos(4x)$.*

close to the Turing bifurcation value $r_T^* \doteq 0.8128$. When $r = 0.68$ is smaller than and far away from the Turing bifurcation value $r_T^*$, the diagonal stripe pattern with ladder pattern near the boundaries is observed as shown in Figure 6(c).

**4.2.2. Memory-delay-induced Hopf bifurcation.** For the delay $\tau > 0$, it follows from Theorem 3.11 that delay-induced Hopf bifurcations appear when $r < r_H^*$. For $d_1 = 0.2, d_2 = 1$, we have $r_T^* \doteq 0.8128, r_H^* \doteq 1.1896$,

$$f_2^H(k) = \frac{4}{5k^2} + \frac{1}{5},$$

and the curves $f_2 = f_2^H(k)$ and $H = H(r_H^*, k)$ are tangent at $k_H^* \doteq 1.4450$, and the curves $f_2 = f_2^T(k)$ and $H = H(r_T^*, k)$ are tangent at $k_T^* \doteq 5.5612$.

Notice that $r_T^* < r_H^*$. It follows from Theorem 3.11 that when $r > r_H^* \doteq 1.1896$, the steady state $u_*$ of (4.1) is always asymptotically stable for any $\tau \geq 0$.

When $r_T^* < r < r_H^*$, there exist delay-induced Hopf bifurcations. For $r = 1 \in (r_T^*, r_H^*)$, the curves $h = H(1,k)$ and $f_2 = f_2^H(k)$ intersect at $k = k_1, k_2$, where $k_1 \doteq 1.1662$ and $k_2 \doteq 2.2078$. For $L = 10$, it follows from $k_1 < n\pi/L < k_2$ that $n = 4, 5, 6, 7$, and the corresponding Hopf bifurcation values $\tau_{n,0}$ are plotted in Figure 7(a). From Figure 7(a), we have

$$\tau_* = \min_{n \in \{4,5,6,7\}} \{\tau_{n,0}\} = \tau_{6,0} \doteq 2.6654.$$

Equation (4.1) undergoes mode-6 Hopf bifurcation at $\tau = \tau_{6,0}$, and the constant steady state $u_* = 1$ is asymptotically stable for $\tau < \tau_{6,0}$ and unstable for $\tau > \tau_{6,0}$. For $\tau = 3$ larger than and close to the Hopf bifurcation value $\tau_{6,0}$, the Hopf bifurcation periodic solution is shown in Figure 8(a). When the memory delay $\tau$ is larger than and far away from the Hopf bifurcation value $\tau_{6,0}$, the numerical simulations have also shown that the spatially inhomogeneous periodic solutions still exist, as shown in Figures 8(b) and 8(c) for $\tau = 30$ and $\tau = 40$, respectively.

**4.2.3. Turing–Hopf bifurcation and double Hopf bifurcation induced by the joint action of the perceptual scale and the memory delay.** In this subsection, we investigate the Turing-Hopf bifurcation and double Hopf bifurcation induced by the joint action of the perceptual scale $r$ and the memory delay $\tau$.

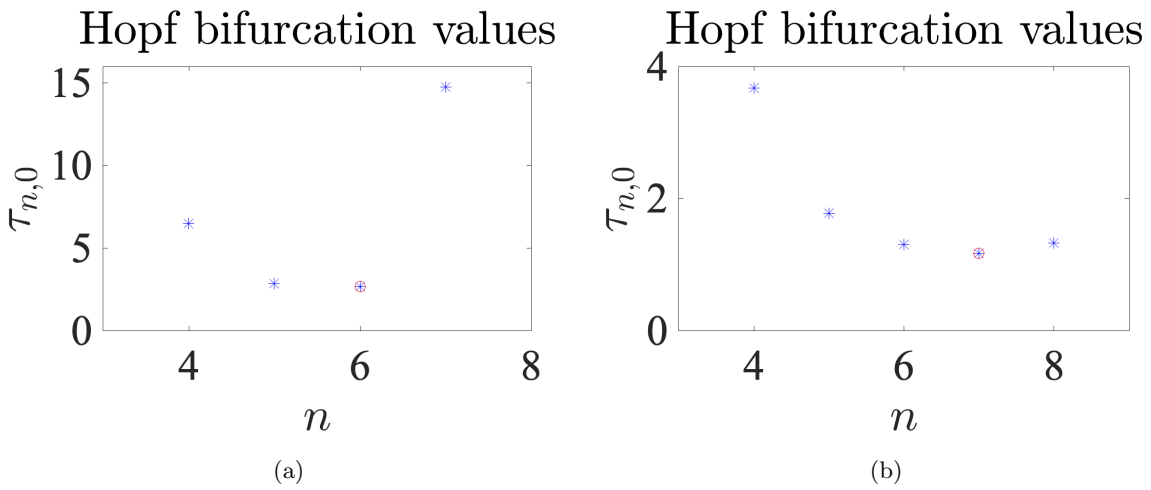


**Figure 7.** *For $d_1 = 0.2$ and $d_2 = 1 > 0$ such that $|\frac{\sin z_2}{z_2}\tilde{d}_2| \le d_1 < |\frac{\sin z_1}{z_1}\tilde{d}_2|$, the critical values $\tau_{n,0}$ of delay-induced Hopf bifurcations for $r_T^* \le r < r_H^*$.* (a) $r = 1 > r_T^*$, $\tau_* = \tau_{6,0}$. (b) $r = r_T^* \doteq 0.8128$, $\tau_* = \tau_{7,0}$.

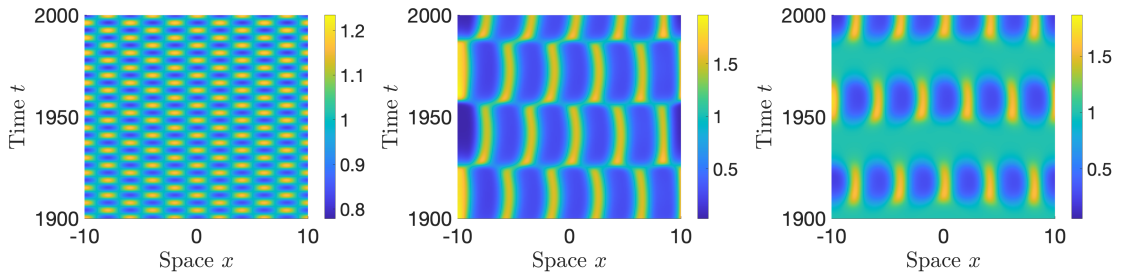


**Figure 8.** *For $d_1 = 0.2, d_2 = 1$, and $r = 1 \in (r_T^*, r_H^*)$, delay-induced periodic patterns of (4.1) for different delays.* (a) $\tau = 3$. (b) $\tau = 30$. (c) $\tau = 40$. *The initial function is chosen as $u(x,t) = u_* + 0.1\cos(4x)$ for $t \in [-\tau, 0]$.*

For $r = r_T^* \doteq 0.8128$, the curves $h = H(r_T^*, k)$ and $f_2 = f_2^H(k)$ intersect at $k = k_1, k_2$, where $k_1 \doteq 1.089$ and $k_2 \doteq 2.9163$, as shown in Figure 5(b). For $L = 10$, it follows from $k_1 < n\pi/L < k_2$ that $n = 4, 5, 6, 7, 8$, and the corresponding Hopf bifurcation values $\tau_{n,0}$ are plotted in Figure 7(b). From Figure 7(b), it is easy to see that

$$\tau_* = \min_{n\in\{4,5,6,7,8\}} \{\tau_{n,0}\} = \tau_{7,0} \doteq 1.1726.$$

From Theorem 3.11, (4.1) undergoes Turing–Hopf bifurcation at $(r, \tau) = (r_T^*, \tau_*)$ arising from the interaction of mode-18 Turing bifurcation and mode-7 Hopf bifurcation. The dotted region in Figure 9 depicts the stable region for the positive constant steady state $u = u_*$ of (4.1).

For $r \in [0.76, 0.92]$ and $\tau \in [0.9, 1.8]$, Figure 9 illustrates the stability region and the critical bifurcation curves. Mode-18 Turing bifurcation (straight line) $r = r_T^*$ and mode-7 Hopf bifurcation (curve line) $\tau = \tau_{7,0}$ intersect at the Turing–Hopf bifurcation point $M_1(r_T^*, \tau_*)$, Mode-7 Hopf bifurcation curve $\tau = \tau_{7,0}$ and mode-6 Hopf bifurcation curve $\tau = \tau_{6,0}$ intersect

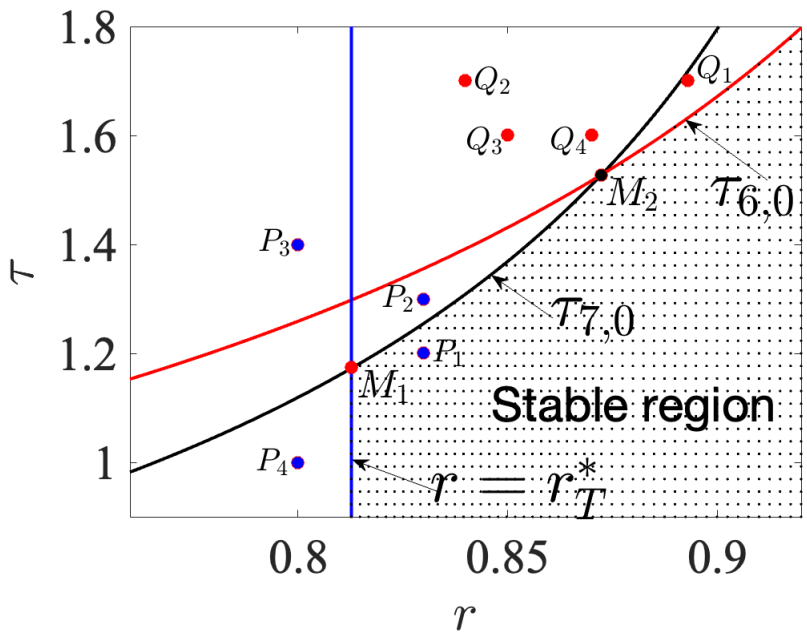


**Figure 9.** *When $d_1 = 0.2$ and $d_2 = 1$, the stable region and the critical bifurcation diagrams of (4.1) in the $r - \tau$ plane for $r \in [0.76, 0.92]$ and $\tau \in [0.9, 1.8]$. $r = r_T^*$ is the mode-18 Turing bifurcation line, $\tau = \tau_{6,0}$ and $\tau = \tau_{7,0}$ are mode-6 and mode-7 Hopf bifurcation curves, respectively. The points are chosen for the numerical simulations; they are $P_1(0.83, 1.2)$, $P_2(0.83, 1.3)$, $P_3(0.8, 1.4)$, $P_4(0.8, 1)$, $Q_1(0.893, 1.7)$, $Q_2(0.84, 1.7)$, $Q_3(0.85, 1.6)$, and $Q_4(0.87, 1.6)$.*

at the double Hopf bifurcation point $M_2(0.8724, 1.5279)$. In the following, we choose different points $P_j$ and $Q_j$, $j = 1, 2, 3, 4$, in Figure 9 to illustrate the spatio-temporal patterns for Turing–Hopf bifurcation and double Hopf bifurcation, respectively.

Figure 10 illustrates the spatio-temporal dynamics of (4.1) for different points $P_j, j = 1, 2, 3, 4$, in the neighborhood of the Turing–Hopf bifurcation point $M_1$. For the point $P_1$, $u_*$ is asymptotically stable, as shown in Figure 10(a). When $\tau$ is increasing across the mode-7 Hopf bifurcation curve $\tau = \tau_{7,0}$, the spatially inhomogeneous periodic solution emerges with spot patterns, as shown in Figure 10(b) for the point $P_2$. For the point $P_3$, Figure 10(c) shows the existence of a spot-stripe pattern. Figure 10(d) illustrates the vertical strip pattern arising from mode-18 Turing bifurcation.

Figure 11 illustrates the spatio-temporal dynamics of (4.1) for different points $Q_j, j = 1, 2, 3, 4$, in the neighbourhood of the double Hopf bifurcation point $M_2$. For the point $Q_1$, Figure 11(a) illustrates the spot patterns arising from the mode-6 Hopf bifurcation. Figures 11(b), 11(c), and 11(d) illustrate the existence of other periodic patterns for the points $Q_2$, $Q_3$, and $Q_4$, respectively.

In what follows, we also numerically investigate the spatio-temporal dynamics of (4.1) when the parameters $\tau$ and $r$ are far away from the boundary of the stable region. For fixed $\tau = 2.5$, Figures 12(a), 12(b), and 12(c) illustrate the dynamics evolution of (4.1) with the

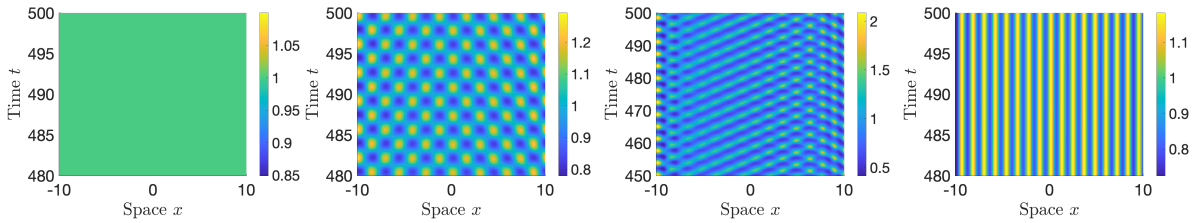


**Figure 10.** *For $d_1 = 0.2, d_2 = 1$, the spatio-temporal dynamics of the solutions of (4.1) for the points $P_j$, $j = 1, 2, 3, 4$, near the neighborhood of Turing–Hopf bifurcation point $M_1$.* (a) $P_1(0.83, 1.2)$. (b) $P_2(0.83, 1.3)$. (c) $P_3(0.78, 1.4)$. (d) $P_4(0.8, 1)$. *The initial function is chosen as $u(x,t) = u_* + 0.1\cos(2x)$ for $t \in [-\tau, 0]$.*

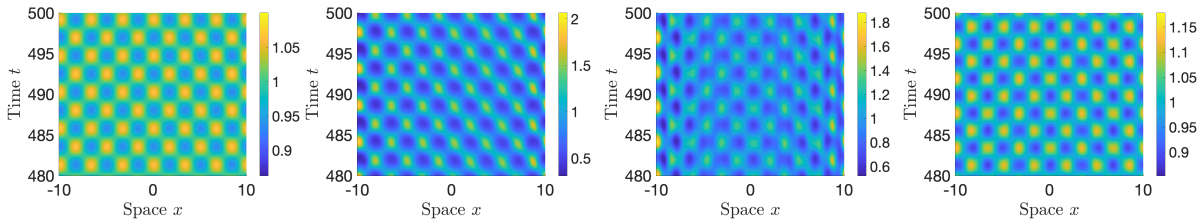


**Figure 11.** *For $d_1 = 0.2, d_2 = 1$, the spatio-temporal dynamics of the solutions of (4.1) for the points $Q_j$, $j = 1, 2, 3, 4$, near the neighborhood of the double Hopf bifurcation point $M_2$.* (a) $Q_1(0.893, 1.7)$. (b) $Q_2(0.84, 1.7)$. (c) $Q_3(0.85, 1.6)$. (d) $Q_4(0.87, 1.6)$. *The initial function is chosen as $u(x,t) = u_* + 0.1\cos(2x)$ for $t \in [-\tau, 0]$.*

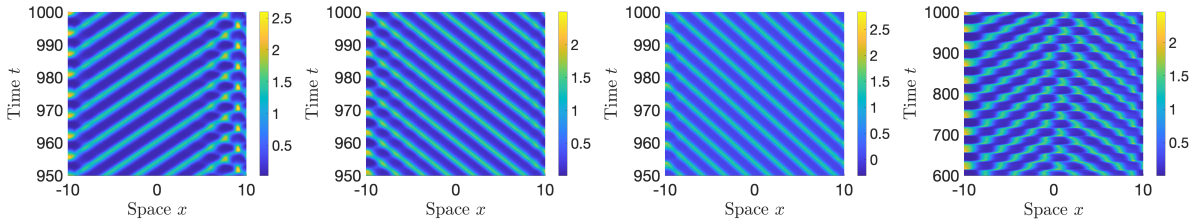


**Figure 12.** *For $d_1 = 0.2, d_2 = 1$, the spatio-temporal dynamics of (4.1) when the parameters $\tau$ and $r$ are far away from the boundary of the stable region.* (a) $r = 0.65, \tau = 2.5$. (b) $r = 0.64, \tau = 2.5$. (c) $r = 0.4, \tau = 2.5$. (d) $r = 0.8, \tau = 20$. *The initial function is chosen as $u(x,t) = u_* + 0.1\cos(2x)$ for $t \in [-\tau, 0]$.*

decreasing of $r$. For $r = 0.65$, Figure 12(a) shows the spot stripe pattern with the stripes leaning to the right. But when $r$ is decreasing to 0.64, a stripe pattern leaning to the left appears, as shown in Figure 12(b). This stripe pattern stays when $r$ is decreasing, as shown in Figure 12(c) for $r = 0.4$. For $r = 0.8$ and large delay $\tau = 20$, a herringbone stripe is observed, as shown in Figure 12(d).

**5. Discussion.** In this paper, we investigate the spatio-temporal dynamics of a reaction-diffusion equation with nonlocal spatial memory. We focus on the influence of nonlocal perceptual scale $r$ and memory delay $\tau$ on the spatially homogeneous positive steady state of (1.3)

and investigate the possible mechanisms driving pattern formation. For the negative memory diffusion rate ($d_2 < 0$), the perceptual scale $r$ and memory delay $\tau$ do not affect the stability of the spatially homogeneous positive steady state. However, for the positive memory diffusion rate ($d_2 > 0$), the perceptual scale $r$ and memory delay $\tau$ can lead to complex dynamics and the appearance of rich patterns. In the following, we conclude our main results and give some discussions for the positive memory diffusion rate.

Without memory (i.e., $\tau = 0$), the influence of the perceptual scale $r$ on the stability of the spatially homogeneous positive steady state depends on the relationship between the random diffusion rate and the memory diffusion rate. When the random diffusion is dominant (i.e., $d_1 \geq |\frac{\sin z_1}{z_1}|\tilde{d}_2$), the perceptual scale $r$ does not affect the stability of the spatially homogeneous positive steady state. When the memory diffusion is dominant (i.e., $d_1 < |\frac{\sin z_1}{z_1}|\tilde{d}_2$), there exists a threshold $r_T^*$ of the perceptual scale such that the spatially homogeneous positive steady state is stable for $r > r_T^*$ and unstable for $0 < r < r_T^*$, and Turing bifurcation occurs at $r = r_T^*$ with the emergence of the spatially inhomogeneous steady state. This implies that when the memory diffusion is dominant, the nonlocal perception is the trigger of the pattern formation. It is surprising that the large perceptual scale does not affect the stability of the spatially homogeneous positive steady state. Our intuitive reason is that a population with a large perceptual radius $r$ has vague information (a small detection function $K_r(x) = \frac{1}{2r}$) over a wide spatial region ($-r \leq x \leq r$), which causes weak perception such that the spatially homogeneous positive steady state is stable. This result also occurs in the other extreme, when the perceptual radius is zero (resulting in no perception over space beyond an animal's own location).

When memory is involved (i.e., $\tau > 0$), the combination of a nonlocal perceptual scale and memory delay can lead to the emergence of complex patterns. When random diffusion is dominant ($d_1 \geq |\tilde{d}_2|$), the nonlocal perceptual scale and memory delay do not affect the stability of the spatially homogeneous positive steady state. When $|\frac{\sin z_1}{z_1}\tilde{d}_2| \leq d_1 < |\tilde{d}_2|$, the memory delay-induced Hopf bifurcation is possible for small perceptual scales ($r < r_H^*$). When $d_1 < |\frac{\sin z_j}{z_j}\tilde{d}_2|$, the combination of a nonlocal perceptual scale and memory delay can lead to Turing–Hopf bifurcation, yielding the existence of spatially inhomogeneous and time-periodic solutions, and to double Hopf bifurcation, yielding more complex patterns. In [6], it has been shown that the occurrence of Turing–Hopf bifurcation is due to symmetry breaking via shifting the step function. In this paper, we show a new mechanism of the occurrence of Turing–Hopf bifurcation by combining a nonlocal perceptual scale and memory delay for the symmetric top-hat function.

Finally, we would also like to mention some challenging problems. It is well known that the normal form theory is an efficient technique to investigate the dynamical classification near the bifurcation point. The algorithms of normal form for Hopf, double Hopf, and Turing–Hopf bifurcations for the reaction-diffusion system with memory-based diffusion have been developed in [29, 27, 26], but we do not know how to calculate the corresponding normal forms taking the perceptual scale $r$ as the bifurcation parameter.

**Data availability.** Data sharing is not applicable to this article as no datasets were generated or analyzed during the current study.

**Conflict of interest statement.** The authors have no competing interests to declare that are relevant to the content of this article.

**Acknowledgments.** The authors are very grateful to two anonymous reviewers for their thoughtful and valuable comments which greatly improved the original manuscript.

## REFERENCES

[1] Q. An, C. Wang, and H. Wang, *Analysis of a spatial memory model with nonlocal maturation delay and hostile boundary condition*, Discrete Contin. Dyn. Syst., 40 (2020), pp. 5845–5868, https://doi.org/10.3934/dcds.2020249.

[2] A. J. Bernoff and C. M. Topaz, *Nonlocal aggregation models: A primer of swarm equilibria*, SIAM Rev., 55 (2013), pp. 709–747, https://doi.org/10.1137/130925669.

[3] A. Buttenschøn and T. Hillen, *Non-local Cell Adhesion Models: Symmetries and Bifurcations in* 1*-D*, Springer, New York, 2021.

[4] J. A. Carrillo, F. James, F. Lagoutiere, and N. Vauchelet, *The Filippov characteristic flow for the aggregation equation with mildly singular potentials*, J. Differential Equations, 260 (2016), pp. 304–338, https://doi.org/10.1016/j.jde.2015.08.048.

[5] L. Chen, K. Painter, C. Surulescu, and A. Zhigun, *Mathematical models for cell migration: A non-local perspective*, Philos. Trans. Roy. Soc. B Biol. Sci., 375 (2020), 20190379, https://doi.org/10.1098/rstb.2019.0379.

[6] A. Ducrot, X. Fu, and P. Magal, *Turing and Turing-Hopf bifurcations for a reaction diffusion equation with nonlocal advection*, J. Nonlinear Sci., 28 (2018), pp. 1959–1997, https://doi.org/10.1007/s00332-018-9472-z.

[7] A. Ducrot and P. Magal, *Asymptotic behaviour of a nonlocal diffusive logistic equation*, SIAM J. Math. Anal., 46 (2014), pp. 1731–1753, https://doi.org/10.1137/130922100.

[8] W. F. Fagan, E. Gurarie, S. Bewick, A. Howard, R. S. Cantrell, and C. Cosner, *Perceptual ranges, information gathering, and foraging success in dynamic landscapes*, Amer. Nat., 189 (2017), pp. 474–489, https://doi.org/10.1086/691099.

[9] V. Giunta, T. Hillen, M. Lewis, and J. R. Potts, *Local and global existence for nonlocal multispecies advection-diffusion models*, SIAM J. Appl. Dyn. Syst., 21 (2022), pp. 1686–1708, https://doi.org/10.1137/21M1425992.

[10] V. Giunta, T. Hillen, M. A. Lewis, and J. R. Potts, *Detecting minimum energy states and multi-stability in nonlocal advection-diffusion models for interacting species*, J. Math. Biol., 85 (2022), p. 56, https://doi.org/10.1007/s00285-022-01824-1.

[11] G. Kaib, *Stationary states of an aggregation equation with degenerate diffusion and bounded attractive potential*, SIAM J. Math. Anal., 49 (2017), pp. 272–296, https://doi.org/10.1137/16M1072450.

[12] T. Laurent, *Local and global existence for an aggregation equation*, Comm. Partial Differential Equations, 32 (2007), pp. 1941–1964, https://doi.org/10.1080/03605300701318955.

[13] S. Li, Z. Li, and B. Dai, *Stability and Hopf bifurcation in a prey-predator model with memory-based diffusion*, Discrete Contin. Dyn Syst. Ser. B, 27 (2022), pp. 6885–6906, https://doi.org/10.3934/dcdsb.2022025.

[14] S. Li, S. Yuan, Z. Jin, and H. Wang, *Bifurcation analysis in a diffusive predator-prey model with spatial memory of prey, Allee effect and maturation delay of predator*, J. Differential Equations, 357 (2023), pp. 32–63, https://doi.org/10.1016/j.jde.2023.02.009.

[15] J. Lin and Y. Song, *Spatially inhomogeneous periodic patterns induced by distributed memory in the memory-based single population model*, Appl. Math. Lett., 137 (2023), 108490, https://doi.org/10.1016/j.aml.2022.108490.

[16] A. Mogilner and L. Edelstein-Keshet, *A non-local model for a swarm*, J. Math. Biol., 38 (1999), pp. 534–570, https://doi.org/10.1007/s002850050158.

[17] D. Morale, V. Capasso, and K. Oelschlager, *An interacting particle system modelling aggregation behavior: From individuals to populations*, J. Math. Biol., 50 (2005), pp. 49–66, https://doi.org/10.1007/s00285-004-0279-1.

[18] K. J. Painter, J. M. Bloomfield, J. A. Sherratt, and A. Gerisch, *A nonlocal model for contact attraction and repulsion in heterogeneous cell populations*, Bull. Math. Biol., 77 (2015), pp. 1132–1165, https://doi.org/10.1007/s11538-015-0080-x.

[19] J. R. Potts and M. A. Lewis, *Spatial memory and taxis-driven pattern formation in model ecosystems*, Bull. Math. Biol., 81 (2019), pp. 2725–2747, https://doi.org/10.1007/s11538-019-00626-9.

[20] J. R. Potts and K. J. Painter, *Stable steady-state solutions of some biological aggregation models*, SIAM J. Appl. Math., 81 (2021), pp. 1248–1263, https://doi.org/10.1137/20M1348066.

[21] H. Shen, Y. Song, and H. Wang, *Bifurcations in a diffusive resource-consumer model with distributed memory*, J. Differential Equations, 347 (2023), pp. 170–211, https://doi.org/10.1016/j.jde.2022.11.044.

[22] J. Shi, C. Wang, and H. Wang, *Diffusive spatial movement with memory and maturation delays*, Nonlinearity, 32 (2019), pp. 3188–3208, https://doi.org/10.1088/1361-6544/ab1f2f.

[23] J. Shi, C. Wang, and H. Wang, *Spatial movement with diffusion and memory-based self-diffusion and cross-diffusion*, J. Differential Equations, 305 (2021), pp. 242–269, https://doi.org/10.1016/j.jde.2021.10.021.

[24] J. Shi, C. Wang, H. Wang, and X. Yan, *Diffusive spatial movement with memory*, J. Dynam. Differential Equations, 32 (2020), pp. 979–1002, https://doi.org/10.1007/s10884-019-09757-y.

[25] Q. Shi, J. Shi, and H. Wang, *Spatial movement with distributed memory*, J. Math. Biol., 82 (2021), 33, https://doi.org/10.1007/s00285-021-01588-0.

[26] Y. Song, Y. Peng, and T. Zhang, *The spatially inhomogeneous Hopf bifurcation induced by memory delay in a memory-based diffusion system*, J. Differential Equations, 300 (2021), pp. 597–624.

[27] Y. Song, Y. Peng, and T. Zhang, *Double Hopf bifurcation analysis in the memory-based diffusion system*, J. Dynam. Differential Equations, (2022), https://doi.org/10.1007/s10884-022-10180-z.

[28] Y. Song, J. Shi, and H. Wang, *Spatiotemporal dynamics of a diffusive consumer-resource model with explicit spatial memory*, Stud. Appl. Math., 148 (2021), pp. 373–395.

[29] Y. Song, S. Wu, and H. Wang, *Spatiotemporal dynamics in the single population model with memory-based diffusion and nonlocal effect*, J. Differential Equations, 267 (2019), pp. 6316–6351, https://doi.org/10.1016/j.jde.2019.06.025.

[30] Y. Song, S. Wu, and H. Wang, *Memory-based movement with spatiotemporal distributed delays in diffusion and reaction*, Appl. Math. Comput., 404 (2021), 126254, https://doi.org/10.1016/j.amc.2021.126254.

[31] C. M. Topaz, A. L. Bertozzi, and M. A. Lewis, *A nonlocal continuum model for biological aggregation*, Bull. Math. Biol., 68 (2006), pp. 1601–1623, https://doi.org/10.1007/s11538-006-9088-6.

[32] C. Wang, S. Yuan, and H. Wang, *Spatiotemporal patterns of a diffusive prey-predator model with spatial memory and pregnancy period in an intimidatory environment*, J. Math. Biol., 84 (2022), 12, https://doi.org/10.1007/s00285-022-01716-4.

[33] H. Wang and Y. Salmaniw, *Open problems in PDE models for knowledge-based animal movement via nonlocal perception and cognitive mapping*, J. Math. Biol., 86 (2023), 71, https://doi.org/10.1007/s00285-023-01905-9.